HHS Public Access

Author manuscript

Dev Cell. Author manuscript; available in PMC 2024 July 24.

Published in final edited form as:

Dev Cell. 2023 July 24; 58(14): 1250–1265.e6. doi:10.1016/j.devcel.2023.05.006.

PLIN5 interacts with FATP4 at membrane contact sites to promote lipid droplet-to-mitochondria fatty acid transport

Gregory E. Miner[1], **Christina M. So**[1], **Whitney Edwards**[1,2], **Joey V. Ragusa**[1], **Jonathan T. Wine**[3], **Daniel Wong Gutierrez**[3], **Michael V. Airola**[3], **Laura E. Herring**[4], **Rosalind A. Coleman**[5], **Eric L. Klett**[5,6,7], **Sarah Cohen**[1,8,*]

[1]Department of Cell Biology and Physiology, University of North Carolina at Chapel Hill, Chapel Hill, North Carolina, 27599, USA (current address for W. Edwards)

[2]Department of Biology, University of North Carolina at Chapel Hill, Chapel Hill, North Carolina, 27599, USA

[3]Department of Biochemistry and Cell Biology, Stony Brook University, New York, 11790, USA

[4]Department of Pharmacology, University of North Carolina at Chapel Hill, Chapel Hill, North Carolina, 27599, USA

[5]Department of Nutrition, University of North Carolina at Chapel Hill, Chapel Hill, North Carolina, 27599, USA

[6]Department of Medicine, University of North Carolina at Chapel Hill, Chapel Hill, North Carolina, 27599, USA

[7]Current address: Department of Medicine, University of Vermont, South Burlington, Vermont, 05403, USA

[8]Lead contact

Summary

Cells adjust their metabolism by remodeling membrane contact sites that channel metabolites to different fates. Lipid droplet (LD)-mitochondria contacts change in response to fasting, cold exposure, and exercise. However, their function and mechanism of formation have remained controversial. We focused on perilipin 5 (PLIN5), a LD protein that tethers mitochondria, to probe the function and regulation of LD-mitochondria contacts. We demonstrate that efficient LD-to-mitochondria fatty acid (FA) trafficking and ß-oxidation during starvation of myoblasts is promoted by phosphorylation of PLIN5 and requires an intact PLIN5 mitochondrial tethering

*Correspondences: Sarah Cohen, sarahcoh@med.unc.edu.

Author Contributions

G.E.M. and S.C. designed the research; G.E.M., C.M.S., W.E., J.V.R., J.T.W., D.W.G., and L.E.H. performed research; G.E.M., C.M.S., W.E., J.V.R., L.E.H., and E.L.K. analyzed data; M.V.A., L.E.H., E.L.K., and R.A.C. provided expertise and feedback, and G.E.M. and S.C. wrote the paper, with input from all co-authors.

Declaration of Interests

The authors declare no competing interests.

domain. Using human and murine cells we further identified the acyl-CoA synthetase, FATP4 (ACSVL4) as a mitochondrial interactor of PLIN5. The C-terminal domains of PLIN5 and FATP4 constitute a minimal protein interaction capable of inducing organelle contacts. Our work suggests that starvation leads to phosphorylation of PLIN5, lipolysis, and subsequent channeling of FAs from LDs to FATP4 on mitochondria for conversion to fatty-acyl-CoAs and subsequent oxidation.

eTOC

Lipid droplets form membrane contact sites with other organelles, including mitochondria, but the function of these contacts has been controversial. Miner et al. show that PLIN5 on lipid droplets interacts with the acyl-CoA synthetase FATP4 on mitochondria to promote fatty acid transport and oxidation in starved myoblasts.

Graphical abstract

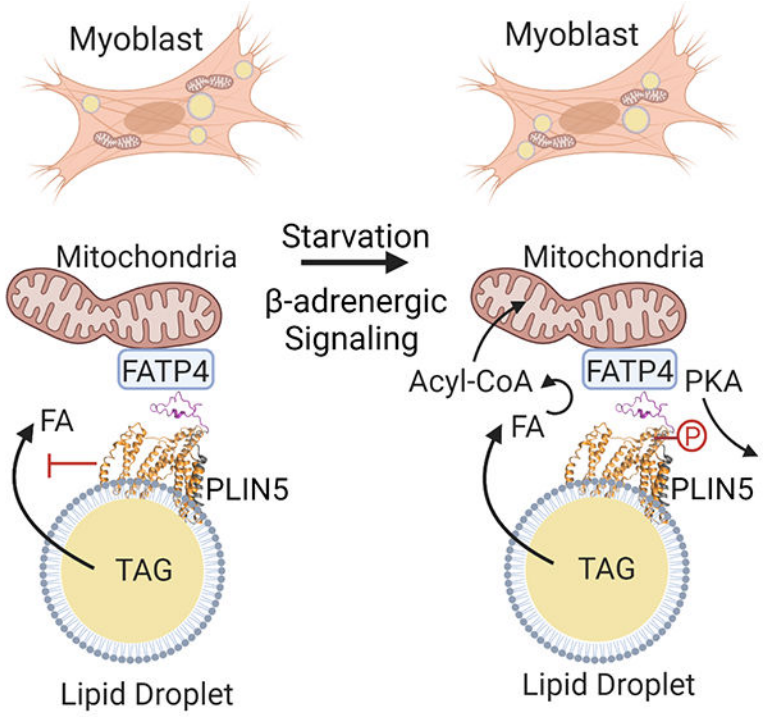

FA:Fatty Acid **TAG**:Triacylglycerol **PKA**:Protein Kinase A **CoA**:Coenzyme A

Keywords

Metabolism; organelles; lipid droplets; mitochondria; membrane contact sites; fatty acids; acyl-CoA; PLIN5; FATP4

Introduction

Cells must adjust their metabolism to respond to changing environmental or developmental cues. An emerging theme is that cells channel metabolites between cellular compartments at

sites of close membrane apposition, called membrane contact sites.[1] These contact sites can be rapidly remodeled in response to signaling cues.[2] In response to starvation, cytoplasmic lipases release fatty acids (FAs) from neutral lipids stored within the primary fat storage organelle, lipid droplets (LDs).[3] FAs are then channeled into mitochondria, where they are oxidized. LD-mitochondria contacts increase in heart and muscle in response to fasting[4] or exercise[5], and in tissue culture cells in response to starvation.[6–9] These observations suggest that membrane contact sites may play a role in channeling lipids from LDs to mitochondria for oxidation. However, the function of contacts between LDs and mitochondria remains controversial. For example, in brown adipose tissue, LD-mitochondria contacts decreased during cold exposure. In this situation, LD-associated mitochondria promoted FA storage rather than oxidation.[10] As a result, multiple roles for LD-mitochondria contact sites have been proposed. These roles include: (1) channeling FAs from LDs to mitochondria for oxidation; (2) channeling FAs or FA breakdown products from mitochondria to LDs to protect mitochondria from lipotoxicity; and (3) channeling ATP from mitochondria to LDs to promote neutral lipid synthesis.[11,12]

Perilipin 5 (PLIN5) is one of only several proteins known to mediate LD-mitochondria contact sites.[13,14] PLIN5 is a member of the conserved family of perilipin LD proteins. It is expressed in highly oxidative tissues including heart, skeletal muscle, and brown adipose tissue[15]. Super-resolution microscopy has localized PLIN5 specifically to sites of apposition between LDs and mitochondria.[16] PLIN5 consists of an N-terminal domain homologous to those of other perilipins, and a unique C-terminal region that recruits mitochondria to LDs.[4] Depletion or overexpression of PLIN5 in mouse models has led to apparently contradictory results. PLIN5-null mice have fewer LDs in heart and muscle[17–20], while overexpression of PLIN5 in the heart leads to cardiac steatosis[21], suggesting a role for PLIN5 in fatty acid sequestration. Consistent with these results, cardiomyocytes cultured from PLIN5-deficient mice more actively oxidized FAs.[17] In contrast, PLIN5 depletion led to reduced FA oxidation in liver[22], while overexpression of PLIN5 in skeletal muscle or brown adipose tissue promoted oxidative gene expression.[23,24] Some of these cell type-specific effects may be explained by the idea that phosphorylation of PLIN5 by protein kinase A can act as a switch between the lipolytic barrier and pro-lipolytic functions of PLIN5.[25,26] Because of these contradictory phenotypes, it has been challenging to untangle the different potential functions of PLIN5. In addition, the mitochondrial protein that PLIN5 interacts with to mediate membrane contact sites has yet to be identified.

Here, we have carefully dissected the lipolytic barrier and tethering functions of PLIN5. By expressing truncated and chimeric protein constructs, we identified a minimal PLIN5 C-terminal domain necessary and sufficient to mediate LD-mitochondria contacts. We further identified FATP4 (ACSVL4), an acyl-CoA synthetase[27], as the mitochondrial binding partner of PLIN5. Chimeric constructs containing the tether domains of PLIN5 or FATP4 were sufficient to create artificial membrane contact sites at the LD-peroxisome or mitochondria-peroxisome interface. Finally, using fluorescent and radioactive FA pulse-chase assays, we show that phosphorylation of PLIN5 at serine 155, an intact PLIN5 mitochondrial tethering domain, and FATP4 expression all promote efficient channeling of FAs from LDs to mitochondria.

Results

PLIN5 contains a C-terminal domain sufficient to mediate LD-mitochondria contacts

In vitro and *in vivo* studies have shown that PLIN5 promotes FA storage in LDs and facilitates membrane contact sites between LDs and mitochondria (LD-mito contacts). The N-terminus of PLIN5 contains a well-characterized lipolytic barrier region that promotes FA storage and is conserved with other perilipins, while the unique C-terminal region is responsible for tethering LDs to mitochondria.[4] Previous studies have demonstrated that expression of a chimeric protein fusing the C-terminal region of PLIN5 (residues 396–463) to PLIN2, a member of the perilipin family, conferred the ability to recruit mitochondria to LDs. Further, it was shown that partial truncation of the C terminus reduces the ability of PLIN5 to induce LD-mito contacts.[4] While the C-terminal region of PLIN5 clearly mediates LD-mito contacts, the mitochondrial binding partner of PLIN5 has not been identified.

To characterize the C-terminal region of PLIN5, we sought to define the specific residues responsible for inducing LD-mito contacts. We first utilized I-TASSER[28–30], a protein structure prediction algorithm that compares primary sequence with known crystal structures, to predict the protein folding of PLIN5. I-TASSER modeling suggested that PLIN5 is composed of two separate structures, an N-terminal region homologous with the lipolytic barrier region of the perilipin family, and a C-terminal domain spanning residues 425–463, which we have termed the tether domain (Fig. 1A). The tether domain has no known closely related crystal structure. Therefore, we utilized QUARK[31,32] *de novo* protein modeling to predict the structure of this domain. QUARK modeling predicts that the tether domain is composed of two α-helices with a hydrophobic pocket (Fig. 1B). Intriguingly, modeling also suggests this hydrophobic pocket may bind lipids, supporting a role in FA trafficking. A recent study[33] demonstrated the ability of recombinant PLIN5 to bind fatty acids, therefore we sought to test whether the C-terminus contains a FA binding domain. We found that both full-length and truncated hPLIN5, lacking half of the C-terminal hydrophobic pocket (hPLIN5CΔ), are capable of binding oleic acid. In contrast to full-length hPLIN5 however, changes to hPLIN5CΔ fluorescence in response to oleic acid were blunted (Fig. S1A,S1B). This suggests that PLIN5 may contain multiple FA binding sites, including one in the C-terminal domain.

To further define the residues comprising the tether domain, we compared the ability of full-length mEmerald tagged PLIN5 (Em-PLIN5) to induce LD-mito contacts with a series of PLIN5 constructs containing successive C-terminal truncations (Em-PLIN5CΔ), guided by our predicted structure (Fig. 1C). As expected, expression of Em-PLIN5 in U-2 OS cells led to a drastic increase in LD-mito colocalization, indicating an increase in membrane contact sites between these organelles. In contrast, cells expressing a C-terminal truncation, PLIN5CΔ (1–424), exhibited no increase in LD-mito colocalization (Fig. 1D,1E). PLIN5 constructs with minimal truncations of the C-terminal domain, as small as 10 amino acids, were also unable to increase LD-mito colocalization. Thus, both predicted α-helices appear to be essential for tether domain function. Importantly, all constructs showed equivalent expression, indicating that observed differences were not caused by variable expression or turnover (Fig. S1C). We also assessed whether the PLIN5 tether domain regulates FA

storage. Expression of Em-PLIN5 and Em-PLIN5CΔ constructs led to equivalent increases in LD area (Fig. 1F). These results suggest that PLIN5 lipolytic barrier function is independent of LD-mito tethering.

To determine if the tether domain alone was sufficient to induce LD-mito contacts, we created PLIN5 constructs lacking the lipolytic barrier region. To maintain LD localization, the lipolytic barrier region of PLIN5 was replaced with the hairpin domain (HP) of GPAT4 (residues 152–208), a minimal domain that allows targeting to LDs without affecting LD physiology[34] (Em-HP-PLIN5C; Fig. 1G,1H). Expression of only the HP domain (Em-HP) demonstrated efficient targeting to the LD, while having no effect on LD-mito contacts (Fig. 1I,1J) or LD area (Fig. 1K). Strikingly, expression of Em-HP-PLIN5C (residues 396–463) significantly induced LD-mito colocalization. Serial truncations of the C-terminal region demonstrated that expression of the entire tether domain, Em-HP-PLIN5C (residues 425–463), is necessary and sufficient to induce LD-mito contacts (Fig. 1J). Further, we observed equivalent expression of all constructs, confirming that differences are not due to variable protein levels (Fig. S1D). We assessed whether inducing LD-mito tethering promotes FA storage in the absence of the lipolytic barrier region. Consistent with the truncation experiments summarized in Fig. 1F, expression of the PLIN5 tether domain did not affect LD area (Fig. 1K). Together, these results show that removal of even 10 amino acids abrogates PLIN5 mitochondrial tether function, thus the whole tether domain (425–463) is required to induce LD-mito contacts.

We next tested the functions of the PLIN5 lipolytic barrier and tether domains in a more oxidative cell type by expressing a subset of these truncation constructs in C2C12 myoblast cells. As in U-2 OS cells, the PLIN5 tether domain was necessary and sufficient to increase LD-mito colocalization, while the lipolytic barrier domain was necessary and sufficient to increase LD area (Fig. S1E,S1G). We further examined the relationship between LD size, contacts with mitochondria, and LD movement. LDs are actively transported along microtubules, both at baseline and in response to changing nutritional conditions.[7,35] We hypothesized that increasing LD-mito contacts by overexpressing PLIN5 would result in reduced LD motion. Indeed, overexpression of full-length PLIN5 significantly slowed LDs in both U-2 OS (Supplemental Movies 1,2) and C2C12 cells (Fig. S1H). Interestingly, expression of either the lipolytic barrier domain (Em-PLIN5CΔ) or tether domain (Em-HP-PLIN5C) alone also slowed LD motion relative to control, with the tether domain having a larger effect (Supplemental Movies 3,4, Fig. S1H). Notably, full-length PLIN5 slowed LDs to a greater extent than Em-PLIN5CΔ or Em-HP-PLIN5C. This indicates that both larger LDs and LDs tethered to mitochondria have reduced motion on microtubules, and that PLIN5 slows LDs via both mechanisms.

These results demonstrate that the PLIN5 tether domain (residues 425–463) is necessary and sufficient to induce LD-mito contacts, and that PLIN5 lipolytic barrier activity is independent of LD-mito tethering. However, both lipolytic barrier and tethering domains of PLIN5 affect LD motion.

PLIN5 phosphorylation and LD-mito contacts drive ß-oxidation by increasing LD-to-mitochondria FA trafficking

We next investigated whether LD-mito contacts promote trafficking of FAs from LDs to mitochondria under starvation conditions using an established pulse-chase assay that visualizes trafficking of the fluorescent FA analog Bodipy 558/568 C_{12} (Red C12) (Fig. 2A).[6] C2C12 myoblasts were treated with trace amounts (5 μM) of Red C12 overnight to allow accumulation in LDs, followed by 1 hr of incubation in complete medium (CM) to remove excess label. Red C12 colocalization with LDs and mitochondria was then monitored immediately before (Fig. 2B, CM) and every 30 min following incubation in Hank's Balanced Salt Solution (HBSS) for 4 hrs. Following incubation in HBSS, cells showed clear relocalization of FAs from LDs to mitochondria (Fig. 2B, S2A).

Protein kinase A (PKA), a crucial regulator of lipolysis, is activated through phosphorylation during fasting.[25] PLIN5 can also be phosphorylated at serine 155 by PKA, resulting in altered interactions with ATGL and its co-activator CGI-58, thereby ablating lipolytic barrier activity and promoting lipolysis.[26,36] Given that lipolysis is required for LD-to-mitochondria FA trafficking, we created full-length and truncated phosphomimetic (S155E) variants of our PLIN5 constructs to investigate the contribution of LD-mito contacts to FA trafficking when lipolysis is active. Previous studies found that expression of PLIN5 constructs with the same mutation replicated effects of PKA-mediated PLIN5 phosphorylation, including changes in cellular localization and transcription.[33,37] However, the ability of this phosphomimetic mutation to ablate lipolytic barrier activity has not previously been demonstrated. We first assessed the effect of phosphomimetic constructs on FA storage. As anticipated, cells expressing PLIN5 showed increased storage of FAs in LDs in response to a Red C12 pulse; in contrast, cells expressing either PLIN5 S155E or PLIN5CΔ S155E showed no significant increase in FA storage, indicating that the phosphomimetic mutation inactivated lipolytic barrier activity (Fig. 2C). We attribute decreased FA storage to altered lipolytic barrier activity, as both PLIN5 S155E and PLIN5CΔ S155E constructs localized appropriately to LDs, affected LD-mito contacts equivalent to PLIN5 and PLIN5CΔ, and were expressed equivalently (Fig. S2B,S2C,S2D).

We then assessed the effect of our PLIN5 constructs on FA trafficking during starvation. Cells overexpressing PLIN5 failed to traffic FAs from LDs to mitochondria after 4 hrs in HBSS, suggesting the lipolytic barrier region was not phosphorylated during the time scale of our assay and thus lipolysis could not occur. Strikingly, cells expressing PLIN5 S155E showed a dramatic increase in FA trafficking to mitochondria under starvation conditions. In contrast, PLIN5CΔ S155E-expressing cells, which have active lipolysis but do not induce LD-mito contacts, showed no significant change in FA trafficking compared to control cells during HBSS incubation (Fig. 2D). These data demonstrate that both PLIN5 phosphorylation and LD-mito contacts function to enhance LD-to-mitochondria FA trafficking under starvation conditions.

To investigate whether the observed effects of PLIN5 expression on FA trafficking led to changes in FA esterification and β-oxidation, we used a modified version of our pulse-chase assay (described above) by using trace amounts (17 μM) of a radioactive FA analog, [1-^{14}C]oleate. Using thin-layer chromatography (TLC), we confirmed incorporation of

[1-^{14}C]oleate into LD-specific neutral lipids, including triacylglycerol (TAG), diacylglycerol (DAG) and cholesterol esters (CE), with TAG being the most abundantly labeled species (Fig. 2E, S2E). Overexpression of PLIN5 led to increased incorporation of [1-^{14}C]oleate into LD-specific neutral lipids, while PLIN5 S155E did not (Fig. 2E). Intriguingly, we observed that overexpression of Em-PLIN5 led to a significant increase in incorporation of [1-^{14}C]oleate into phosphatidylserine (PS). Membrane contact sites between ER and mitochondria facilitate PS transport into mitochondria, where PS is subsequently converted to phosphatidylethanolamine (PE).[38] We therefore hypothesized that PLIN5 overexpression may promote LD-mito contact sites at the expense of ER-mito contacts and thereby inhibit the transport and subsequent conversion of PS to PE. Consistent with this we found that PLIN5 overexpression led to a significant reduction in ER-mito contact sites (Fig. S2F,S2G). To assess β-oxidation, we measured the amount of ^{14}C acid soluble molecules (ASM) released from cells following nutrient starvation. Mirroring our FA trafficking assay, we found that expression of Em-PLIN5 did not change β-oxidation compared to control. In contrast, expression of Em-PLIN5 S155E significantly increased β-oxidation relative to control and Em-PLIN5. Finally, expression of the truncated phosphomimetic PLIN5CΔ S155E failed to increase β-oxidation relative to control and showed reduced β-oxidation compared to PLIN5 S155E (Fig. 2F).

Previous work has shown that, over extended time periods, overexpression of PLIN5 S155E can promote transcription of genes that mediate mitochondrial biogenesis and oxidative function, including carnitine palmitoyltransferase I (CPT1).[37] Increased protein expression of CPT1 has the potential to affect FA transport into mitochondria and β-oxidation. However, on the time scale of our assays (cells transfected for 24 hrs followed by 4 hrs of starvation), expression of PLIN5 S155E did not significantly increase levels of CPT1 protein (Fig. S2H). This indicates the effects of expressing PLIN5 S155E in our assays should be attributed to protein-protein interactions and LD-mitochondrial tethering, and not to transcriptional effects.

Together, these data demonstrate that PLIN5-induced LD-mito contacts enhance the trafficking of FAs from LDs to mitochondria during starvation, leading to increased β-oxidation. This activity is promoted by a phosphomimetic mutation of the PLIN5 lipolytic barrier region, suggesting that PLIN5 mediates the metabolic shift from glycolysis to β-oxidation by regulating both lipolysis and FA trafficking.

The PLIN5 tether domain interacts with acyl-CoA synthetase FATP4

Our studies thus far have established a physiological consequence of LD-mito contacts induced by the tether domain of PLIN5. However, the mechanisms by which these contacts form remains unclear. We hypothesized that the tether domain of PLIN5 interacts with one or more outer mitochondria membrane (OMM) proteins. To identify protein interactions specific to the tether domain of PLIN5, we performed affinity purification-mass spectrometry (AP-MS) with cells expressing either Em-PLIN5 or Em-PLIN5CΔ. To understand the contribution of the two predicted α-helices (Fig. 1B) to protein binding, we utilized Em-PLIN5CΔ constructs lacking either a single helix (Em-PLIN5CΔ(1–443)) or both (Em-PLIN5CΔ(1–424)). Em-PLIN5 and Em-PLIN5CΔ protein complexes were affinity

purified from transfected U-2 OS cells using a high-affinity nanobody for GFP (GFP-Trap). As a control, affinity purification was performed using cells transfected with mEmerald alone (Em). Affinity-purified proteins were then analyzed by LC-MS/MS on a QExactive HF mass spectrometer. Two independent biological replicates were analyzed in duplicate. Proteins were considered putative PLIN5 interactors if they showed 2-fold enrichment over control and were detected by at least 2 peptides in both biological replicates. Putative interactors were then analyzed using SAINT (Significance Analysis of INTeractome)[39] to identify PLIN5 interactors with high confidence.

A total of 59 putative PLIN5 interactors passed our statistical cutoffs (Supplemental Table 1). Of these, 24 showed decreased abundance in both of our affinity-purified PLIN5 CΔ protein complexes (Fig. 3A,3B) suggesting they interact specifically with the tether domain of PLIN5. For most tether-specific interactors (19/24), we found that full truncation of the tether domain led to a 2-fold or greater reduction in protein binding relative to partial truncation, suggesting the α-helix spanning residues 425–443 may be primarily responsible for protein-protein interactions. We identified two proteins that were of particular interest due to their mitochondrial localization and role in in FA metabolism: FATP4 and ACOT9. Because ACOT9 is primarily localized to the inner mitochondrial membrane[40], we deemed that it was unlikely to facilitate organelle tethering, though this data may suggest the formation of a complex spanning mitochondrial membranes. FATP4 is an OMM bifunctional Acyl-CoA synthetase (ACSVL) that has FA transport and acyl-CoAs synthetase activity, with substrate preference towards C16-C24 FAs [41]. FATP4 has also been implicated in promoting β-oxidation through re-esterification of long chain FAs following lipolysis.[42–44] Related ACSL proteins, such as ACSL1, have been shown to associate with LD tethering proteins such as SNAP23[45], supporting a potential role in mediating LD-mito contacts. Further, exercise increases expression of both PLIN5[46] and FATP4[47], which may be primarily responsible for the observed increase in LD-mito contacts.[48,49]

Western blot analysis of our affinity-purified PLIN5 complexes confirmed that FATP4 interacts with the tether domain of PLIN5 (Fig. 3C). Though it did not appear in our AP-MS screen, mitofusin 2 (MFN2) has recently been implicated as a potential LD-mito tether through interaction with PLIN1.[50] Because the lipolytic barrier domains of PLIN1 and PLIN5 are conserved, we tested whether PLIN5 interacts with MFN2 and found that this is, indeed, the case. However, in contrast to FATP4, MFN2 binding to PLIN5 does not decrease upon truncation of the tether domain (Fig. 3C,3D). This indicates that MFN2 interacts with both PLIN1 and PLIN5 via the homologous lipolytic barrier region.

PLIN5 and FATP4 drive membrane contact site formation

Given that FATP4 interacts specifically with the PLIN5 tether domain, we next investigated whether these proteins constitute a minimal protein interaction sufficient to drive membrane contact sites. If these proteins constitute a minimal membrane tether, they should be capable of inducing contact sites in the absence of additional LD or mitochondrial proteins. To test this possibility, we first assessed whether recruitment of the PLIN5 tether domain to peroxisomes could induce peroxisome-mitochondria contact sites. We adapted our LD-targeted construct design by replacing the HP domain with the peroxisomal

membrane protein targeting sequence (residues 1–33) of PEX3 (Pex) to localize the PLIN5 tether domain to peroxisomes (Pex-Em-PLIN5C) (Fig. 4A,4B). Expression of control constructs containing only mEmerald tagged Pex (Pex-Em) in U-2 OS cells showed efficient recruitment to peroxisomes but no apparent effect on peroxisome-mitochondria colocalization. In contrast, expression of Pex-Em-PLIN5C significantly increased peroxisome-mitochondria colocalization (Fig. 4C,D). Expression of Pex-Em-PLIN5C did not affect peroxisome area relative to control (Fig. S3A). These results suggest that the PLIN5 tether domain drives membrane contact site formation independent of the unique membrane architecture of the LD.

We next assessed whether HP-Em-PLIN5C can induce contact sites with FATP4 relocalized to the peroxisomal membrane. FATP4 is an integral membrane protein containing a large cytosolic C-terminal domain (156–643)[51], which we hypothesized contained the PLIN5 interaction site. For these experiments, we created constructs that localize the C-terminal domain of FATP4 (FATP4C) to the peroxisomal membrane (Pex-BFP-FATP4C) (Fig. 4E,4F). Co-expression of Em-HP-PLIN5C and Pex-BFP-FATP4C showed an approximately 2-fold increase in LD-peroxisome colocalization compared to controls transfected with only membrane-targeting sequences (Em-HP and Pex-BFP). In contrast, expression of Em-HP-PLIN5C or Pex-BFP-FATP4C alone did not increase LD-peroxisome colocalization (Fig. 4G,4H). Expression of these constructs, either alone or together, did not affect LD or peroxisome area (Fig. S3B,S3C). Together, these data suggest that the PLIN5 tether domain and FATP4 C-terminal domain form a minimal protein interaction sufficient to drive membrane contact sites. Further, the ability to relocalize either protein while retaining contact site induction suggests that additional resident LD or mitochondrial proteins are not required for this activity.

Loss of FATP4 impairs PLIN5 induced LD-mito contacts and FA trafficking

Recent work has shown that many membrane contact sites utilize multiple tethers, and loss of a single tether may not drastically alter contact site formation.[52] Having shown that PLIN5 and FATP4 can interact to induce membrane contact sites, we next tested whether FATP4 is required for PLIN5-driven LD-mito contacts by depleting FATP4. FATP4 expression in C2C12 myoblasts was inhibited by siRNA transfection (FATP4 siRNA), leading to a >70% reduction in FATP4 protein abundance relative to non-targeting siRNA (NT siRNA) (Fig. S4A,S4B). Expression of Em-PLIN5 in FATP4-knockdown cells showed an ~50% reduction in LD-mito contacts relative to NT siRNA controls (Fig. 5A,5B). The inability of FATP4-knockdown to fully ablate Em-PLIN5 induction of LD-mito contacts suggests there may be additional PLIN5 binding partners on the mitochondrial membrane that facilitate LD-mito contacts. Alternatively, this may be due to incomplete knockdown of FATP4, as our results indicate that 10–30% of FATP4 remained following FATP4 siRNA knockdown. In contrast, loss of FATP4 did not appear to affect PLIN5 lipolytic barrier function, as expression of Em-PLIN5 increased LD area in FATP4-knockdown cells comparable to NT siRNA treated cells (Fig. 5C).

Next, using the pulse-chase assay shown in Fig. 2A, we investigated whether the loss of FATP4 alters the ability of PLIN5 to facilitate LD-to-mitochondria FA trafficking during

starvation. After Red C12 pulse, FATP4-knockdown cells transfected with phosphomimetic PLIN5 S155E stored a similar amount of Red C12 within LDs compared to NT siRNA treated cells (Fig. 5D). Upon starvation, however, FATP4-depleted cells expressing PLIN5 S155E were unable to efficiently traffic FAs to mitochondria (Fig. 5E). Interestingly, loss of FATP4 completely ablated PLIN5 S155E-induced FA trafficking while only partially preventing LD-mito contacts (Fig. 5B,5E). This indicates that FATP4 not only serves as a LD-mito tether but may also directly facilitate FA trafficking through its ACSL activity.

Endogenous PLIN5 and FATP4 induce LD-mito contacts and FA transfer in response to β-adrenergic signaling

Our data demonstrate that the tether domain of PLIN5 interacts with FATP4 to induce LD-mito contacts and facilitate trafficking of FAs from LDs to mitochondria during nutrient starvation, promoting β-oxidation. We next sought to determine if endogenous induction of PLIN5 recapitulates these findings. Recently it was demonstrated that activation of the β-adrenergic/PKA pathway in C2C12 myotubes, through treatment with isoproterenol (ISO) and 3-isobutyl-1-methylxanthine (IBMX), induces endogenous PLIN5 expression and PKA-dependent phosphorylation of PLIN5 at serine 155.[37] To test the consequences of endogenous PLIN5 induction and phosphorylation on LD-mito contacts and LD-to-mitochondria FA trafficking, we treated C2C12 myoblasts with ISO-IBMX. Following overnight ISO-IBMX treatment, mRNA expression of PLIN5 significantly increased (Fig. S5A). As expected, induction of endogenous PLIN5 expression by ISO-IBMX resulted in a significant increase in LD-mito interactions relative to vehicle controls (Fig. 6A,6B). Induction of LD-mito interactions by ISO-IBMX was accompanied by a decrease in ER-mito contacts as seen with PLIN5 overexpression (Fig. S5B,S5C). ISO-IBMX had no effect on LD area, consistent with phosphorylation of PLIN5 at serine 155 by PKA (Fig. S5D,6C). Crucially, cells depleted of PLIN5 by siRNA transfection (PLIN5 siRNA), which blunts ISO-IBMX induction of PLIN5 (Fig. S5E), did not increase LD-mito contacts in response to ISO-IBMX treatment. Further, FATP4-depleted cells also failed to induce LD-mito contacts in response to ISO-IBMX (Fig. S5D,6B).

Finally, we assessed whether induction of PLIN5/FATP4-dependent LD-mito contacts by ISO-IBMX altered LD-to-mitochondria FA trafficking during starvation. As seen with PLIN5 S155E overexpression, induction and phosphorylation of PLIN5 by ISO-IBMX did not affect the amount of Red C12 stored within LDs following the Red C12 Pulse (Fig. 6D). In response to starvation, cells treated with ISO-IBMX showed significantly increased FA trafficking to mitochondria relative to cells treated with vehicle (Fig. 6E). As expected, disruption of ISO-IBMX induced LD-mito contacts through depletion of PLIN5 or FATP4 ablated the ability of cells to efficiently traffic FAs. These findings suggest that induction of LD-mito contacts and LD-to-mitochondria FA transfer by β-adrenergic requires both endogenous PLIN5 expression/phosphorylation and FATP4.

Discussion

We have focused on the LD protein PLIN5 to investigate the function and mechanism of formation of LD-mito contact sites. We used predictive modeling and expression of

truncated and chimeric protein constructs to precisely identify a minimal PLIN5 C-terminal domain required for tethering to mitochondria (amino acids 425–463; Fig. 1). The creation of a truncation construct lacking this domain allowed us to identify an acyl-CoA synthetase, FATP4, as the mitochondrial binding partner of PLIN5 by using co-immunoprecipitation/mass spectrometry (Fig. 3). Chimeric constructs containing the C-terminal tether domains of PLIN5 and FATP4 were sufficient to create membrane contacts at the LD-peroxisome or mitochondria-peroxisome interface (Fig. 4). We used fluorescent and radioactive FA pulse-chase assays to test the function of LD-mito contacts during starvation of C2C12 myoblast cells. We found that phosphorylation of PLIN5 at serine 155, an intact PLIN5 mitochondrial tethering domain, and expression of FATP4 all promote efficient channeling of FAs from LDs to mitochondria and subsequent β-oxidation in response to starvation (Fig. 2,5,6). We propose that during starvation: (1) PKA phosphorylates PLIN5 at serine 155[26]; (2) phosphorylation of PLIN5 promotes lipolysis of triacylglycerol and release of FAs[25,36,53]; (3) released FAs are channeled from LDs to mitochondria at membrane contact sites, where FATP4 converts FAs to fatty-acyl-CoAs, enabling; (4) transport into mitochondria for β-oxidation (Fig. 6F).

Our *de novo* modeling and *in vitro* FA binding assay suggest that the PLIN5 tether domain contains a hydrophobic pocket that binds FAs (Fig. 1B, S1A). PLIN5 has previously been shown to bind FAs, with lipid binding regulated by phosphorylation[33]. Our data imply that FA binding occurs in both the tether and lipolytic barrier regions of PLIN5. It is possible that N-terminal lipid binding drives association of PLIN5 with LDs, while our identified lipid-binding pocket in the tether domain transfers FAs from LDs to mitochondria. However, further experiments are needed to test the ability of the PLIN5 C-terminal domain to transfer lipids between membranes.

The presence of acyl-CoA synthetases (ACSLs) at LD-organelle contact sites is an emerging theme. For example, ACSL1 on mitochondria interacts with LD-tethering proteins including SNAP23[45]. Intriguingly, ACSL1 localization at mitochondria appears to be regulated by TANK-Binding Kinase 1 in response to fasting. Relocalization of ACSL1 to mitochondria subsequently increases β-oxidation[54]. Similarly, the ER-LD tethering protein SNX14 interacts with ACSL4 [55], an isoenzyme of which localizes to ER/LDs[56]. ACSL3 has been localized at the ER membrane microdomains responsible for LD biogenesis, as well as on emerging and mature LDs[57], suggesting that ACSL3 may also be present at ER-LD contact sites. The presence of ACSLs at LD-organelle contact sites indicates a prominent role for these membrane contact sites in channeling fatty acids to different metabolic fates.

What is the function of PLIN5-mediated LD-mito contacts? Multiple functions have been proposed, based on seemingly contradictory results from mouse and cell models of PLIN5 ablation or overexpression. Our results are consistent with previous work showing that PLIN5 can switch between lipolytic barrier and pro-lipolytic activities, depending on its phosphorylation state.[25,26] Our findings are also consistent with recently published work showing that expression of truncated PLIN5 in human AC16 cardiomyocytes does not alter ß-oxidation relative to full-length PLIN5 during acute starvation.[58] Because that study did not use phosphomimetic PLIN5 constructs, the authors concluded that the PLIN5 mitochondrial tether domain is dispensable for FA oxidation. Here we have used

a combination of phosphomimetic and truncation constructs to carefully tease apart the roles of the PLIN5 lipolytic barrier and mitochondria tether domains. While the PLIN5 lipolytic barrier domain can promote either FA storage or mobilization depending on its phosphorylation state, we found that the PLIN5 mitochondrial tether domain was required for efficient flux of FAs from LDs to mitochondria, and their subsequent oxidation. Thus, we propose that a primary function of PLIN5-mediated LD-mito contacts is to efficiently channel FAs from LDs to mitochondria. This occurs through interaction of the PLIN5 C-terminal domain with FATP4. Interestingly, LD-to-mitochondria FA flux was completely ablated by knockdown of FATP4, while LD-mito colocalization was reduced but not abolished by FATP4 depletion (Fig. 5). This implies that additional mitochondrial proteins such as the recently identified PLIN5 interactor Rab8a[59] may interact with PLIN5 at membrane contact sites, but that the FATP4 interaction is specifically required for FA channeling. Indeed, we observed an interaction between the PLIN5 lipolytic barrier domain and the mitofusin MFN2 (Fig. 3). MFN2 was previously reported to interact with PLIN1, which shares a conserved N-terminal domain with PLIN5.[50] Thus, PLIN5-mediated LD-mito contacts may have additional functions beyond FA channeling, including the regulation of mitochondrial fusion. Whether the interaction of PLIN5 with binding partners, including FATP4 and MFN2, occurs at the same or distinct membrane microdomains remains to be determined. The spatial relationship between PLIN5/FATP4 and other LD-mito contact proteins including SNAP23/ACSL1[45,60], MIGA2[61], and VPS13D/TSG101[62], is also an area of future investigation.

The channeling of FAs directly from LDs to mitochondria at membrane contact sites during starvation has the benefit of preventing a build-up of cytoplasmic FAs, which can lead to mitochondrial toxicity.[8] Alternative FA trafficking routes from LDs to mitochondria have been proposed. Previous work has suggested that the primary route in hepatocytes is through lipophagy of LDs, followed by fusion of lysosomes with the plasma membrane and subsequent reuptake of FAs and transport to mitochondria.[63] Like FA transfer at LD-mito contact sites, lysosomal fusion with the plasma membrane would also prevent a buildup of cytoplasmic FAs, by releasing FAs extracellularly and enabling regulation of cytoplasmic FA concentration at the reuptake step. Which mechanism is used likely depends on the cell-type specific expression of regulatory proteins, as well as the stimulus that initiates lipolysis versus lipophagy.

In summary, we have identified the acyl-CoA synthetase FATP4 as an interactor with PLIN5. We provide evidence that PLIN5 interacts with FATP4 at LD-mito contact sites to promote LD-to-mitochondria trafficking of FAs. This work helps to reconcile seemingly contradictory results seen in models of PLIN5 ablation/overexpression by revealing the specific functions of the lipolytic barrier vs. mitochondrial tethering domains of PLIN5.

Limitations of the Study

Our studies provide evidence that the mitochondrial tether domain of PLIN5 interacts with FATP4 to drive membrane contact sites in cultured U-2 OS and C2C12 cells. Further, PLIN5-FATP-mediated contacts promote LD-to-mitochondria fatty acid trafficking in response to starvation or ß-adrenergic signaling. A limitation of this study is the use of

immortalized cell lines. While our functional studies utilized a C2C12 myoblast cell line to assess the role of the PLIN5-FATP4 interaction in skeletal muscle, future experiments using an *in vivo* model will be necessary to fully elucidate the physiological functions of these contacts. Further, our experiments assessing the effects of ß-adrenergic signaling required chemical induction, which may not fully recapitulate physiological conditions. Future use of an *in vivo* system will allow direct investigation of relevant conditions such as starvation, exercise, and cold exposure in multiple cell types.

Resource Availability

Lead Contact

Further information and requests about resources and reagents are available from the corresponding author, Sarah Cohen (sarahcoh@med.unc.edu), upon reasonable request.

Materials availability

Plasmids generated in this study will be made available from the lead contact on request.

Data availability

The mass spectrometry proteomics data generated and analyzed during the current study have been deposited to the ProteomeXchange Consortium via the PRIDE [64] partner repository with the dataset identifier PXD031591.

Any additional information required to reanalyze the data reported in this paper is available from the lead contact upon reasonable request.

Experimental model and subject details

U-2 OS cells and C2C12 myobolasts were obtained from the UNC Tissue Culture Facility and maintained in Dulbecco's Modified Eagle Medium (DMEM) with 10% FBS and 4 mM glutamine (complete medium, CM). Cells were cultured on chambered cover glass (#1.5 high performance cover glass, Cellvis), coated with 10 μg/ml fibronectin (MilliporeSigma). For starvation experiments, Hank's buffered salt solution (HBSS, 14025092) was purchased from Thermo Fisher.

Method details

Cell transfection

Cells were transfected with Mito-RFP[65], Mito-GFP[66], mOrange-SKL[9], mApple-Sec61b[67], or PLIN5 constructs using Lipofectamine 2000 (Invitrogen), according to the manufacturer's instructions. RNA interference was performed using 25 nM ON-TARGETplus Mouse FATP4 (J-063631–12-0002) siRNA, ON-TARGETplus mouse PLIN5 siRNA SMARTPOOL (L-055756–01-0005) or ON-TARGETplus non-targeting pool (Horizon Discovery) and DharmaFECT 1 (Horizon Discovery), according to the manufacturer's instructions.

Plasmids

Full-length PLIN5, PLIN5 truncations and Chimeric PLIN5 or FATP4 constructs were generated using HiFi DNA Assembly Master mix (New England Biolabs, E2621). PLIN5 mutant constructs were generated using a Q5® Site-Directed Mutagenesis Kit (New England Biolabs, E0554S); and mEmerald-C1 and BFP-KDEL were used as vectors for mEmerald- and TagBFP- tagged constructs, respectively. Human perilipin 5 (hPLIN5) was gene synthesized (BioBasic, Canada) into ppSUMO, which added a ULP-1 cleavable N-terminal His-tagged SUMO protein (ppSUMO-hPLIN5). hPLIN5CΔ construct (residues 1–424) in ppSUMO (ppSUMO-hPLIN5CΔ) was generated using KLD enzyme mix (New England BioLabs, M0554S). For plasmid construction, all PCRs were performed using Q5 High Fidelity DNA polymerase (M0419; New England Biolabs) and restriction enzymes from New England Biolabs. The following plasmids were kind gifts: pEYFP-C1-PLIN5 from Carole Sztalryd (University of Maryland)[4]; TagBFP-KDEL from Gia Voeltz (University of Colorado) [68]; mEmerald-C1 and mOrange-SKL from Michael Davidson (Florida State University) [69]; Mito-GFP, Mito-RFP, and mApple-Sec61b from Jennifer Lippincott-Schwartz (Janelia Research Campus).

Inhibitors and antibodies

The following chemicals, dyes and antibodies were used: 10 μg/ml fibronectin (MilliporeSigma), 5 μM BODIPY 558/568 C12 (Life Technologies), 5 nM [1-^{14}C]oleate (Perkin Elmer), 50 ng/ml BODIPY 665/676 (Life Technologies), 100 nM MitoTracker Deep Red (Life Technologies), L-carnitine (Thermo Fisher), bovine serum albumin-fatty acid free (MilliporeSigma), anti-CPT1B (Abcam, ab104662), anti-GFP (Invitrogen, A10262), anti-FATP4 (Abcam, ab200353), anti-Mfn2 (Cell Signaling, 11925), and anti-β-tubulin (Cell Signaling Technologies, 2146).

Protein expression and purification

hPLIN5 and hPLIN5CΔ plasmids were expressed in Escherichia coli BL21 (DE3) RIPL cells. Cells were grown at 37 °C in Ultra-High Yield Flasks (Thompson Instrument Company) to an OD600nm of 1.5 and then cooled at 30 °C for 30 min. Protein expression was induced with isopropyl β-D-1-thiogalactopyranoside (IPTG) at 30 °C for 3 h, cells were harvested by centrifugation, and stored at −80 °C.

Frozen cells were resuspended in buffer A (50 mM Tris-HCl, 500 mM NaCl, 5 mM imidazole, 5% (v/v) glycerol, 1% (w/v) n-dodecyl-β-D-maltoside (DDM) (GoldBio), 10 mM 2-mercaptoethanol (β-ME) (Sigma), pH 7.5) containing leupeptin (10 μg in sterile H2O), aprotinin (1 μg in PBS), and pepstatin (10 μg in 9% EtOH, 10% DMSO), lysed by sonication, and centrifuged at 81,770 × g at 4 °C for 1 h. The resulting supernatant was incubated at 4 °C for 12 hr with pre-equilibrated Ni-NTA resin (GoldBio) and applied to a gravity column. The column was washed with buffer B (50 mM Tris, 500 mM NaCl, 50 mM imidazole, 5% (v/v) Glycerol, 0.2% (w/v) DDM, 10 mM β-ME, pH 7.5) and protein was eluted with buffer C (50 mM Tris, 500 mM NaCl, 300 mM imidazole, 5% (v/v) Glycerol, 0.2% (w/v) DDM, 10 mM β-ME, pH 7.5). The eluted protein was incubated at 4 °C for 12 h with ULP-1 to cleave the His-SUMO fusion and applied to a HiLoad Superdex 200 26/600 200pg column (GE Healthcare) equilibrated with Buffer T (20 mM Tris, 100 mM NaCl,

0.2% (w/v) DDM, 10 mM β-ME, pH 7.5). Pooled fractions from SEC were concentrated to 0.5–1.5 mg/ml using a 10kDa MWCO concentrator and applied to a Superdex 200 Increase 10/300 GL column (GE Healthcare) equilibrated with Buffer P (10 mM NaH2PO4, 100 mM NaCl, 10 mM β-ME, pH 7.5). Pooled fractions from SEC were supplemented with 10 mM DTT, concentrated to 0.5–1.3 mg/ml using a 10 kDa MWCO concentrator, aliquoted, flash frozen in liquid nitrogen, and stored at −80 °C.

Tryptophan fluorescence binding assay

Lipid binding to purified protein was assessed by measuring tryptophan fluorescence quenching following incubation with oleic acid. Briefly, recombinant protein (800nM in 150 nM in 10 mM NaH2PO4, pH 7.5) was incubated with buffer or oleic acid for 30 min at room temperature in a black 96 well glass bottom plate (Cellvis, P96–1.5H-N). Intrinsic tryptophan fluorescence of purified protein was then measured at 350 nm following excitation at 295 nm using a Cytation 5 Imaging Multi-Mode Microplate Reader (BioTek). Background fluorescence resulting from buffer and ligand was corrected for each concentration of oleic acid.

Fluorescent FA analog pulse-chase

C2C12 cells were incubated with CM containing 5 μM BODIPY 558/568 C12 (Red C12, Life Technologies) for 16 hr. Cells were then washed three times with CM, and chased for 1 hr in order to allow the fluorescent lipids to incorporate into LDs. Cells were imaged immediately following pulse-chase labeling with Red C12. Cells were then washed three times with HBSS and imaged every 30 min for 4 hrs in order to track the subcellular localization of FAs. To visualize mitochondria, cells were transfected with Mito-GFP 24 hrs prior to Red C12 labeling. To label LDs, Bodipy 665/676 (Life Technologies) was added to cells at 50 ng/ml 16 hrs prior to imaging and was present during imaging.

Radioactive FA pulse-chase

C2C12 cells were incubated with Krebs-Ringer bicarbonate HEPES (KRBH) labeling buffer (KRBH containing 5.5 mM glucose, 1mM carnitine, 0.25% FA free BSA) and 17 μM [1-^{14}C]oleate (^{14}C-oleate, Perkin Elmer) for 16 hrs. Cells were then washed three times with KRBH, and chased for 1 hr in KRBH labeling buffer in order to allow ^{14}C-oleate incorporation into cellular lipids. Following the pulse-chase, cells were either collected to measure ^{14}C-oleate incorporation, or incubated in HBSS to assess β-oxidation.

β-Adrenergic activation

C2C12 cells were incubated with 10μM Iso and 500μM IBMX for 18hrs to induce β-adrenergic signaling.

Lipid extraction and TLC

Following the Radioactive FA pulse-chase, cells were washed twice with KRBH containing 1% FA Free BSA. Lipids were isolated by chloroform-methanol extraction. Following extraction, lipids were dried by speedvac and resuspended in chloroform-methanol. Aliquoted samples were counted for total ^{14}C-oleate incorporation. Remaining

samples were spotted onto preparative silica gel TLC plates (MilliporeSigma). Separation of lipids was accomplished by developing the plates in a 2-step solvent system of chloroform:methanol:ammonium hydroxide, 65:25:4 (vol/vol) followed by heptane:isopropyl ether:acetic acid (15:10:1) (vol/vol). Radiolabeled samples were visualized using a Bioscan AR-2000 radio-TLC imaging scanner (Bioscan).

ASM measurement

Following Radioactive FA pulse-chase, cells were washed three times with HBSS and incubated with HBSS containing 1 mM carnitine. 500 µl of media was collected after 6 hrs and incubated with 12.5 µl of 25% FA-free BSA overnight at 4 °C followed by centrifugation at 20,800 gfor 20 min. Supernatants were washed once more with 12.5 µl of 25% FA-free BSA and spun at 20,800 g for 20 min, before aliquots of the supernatant were counted for ^{14}C-labeled ASM.

Isolation of GFP-PLIN5 complexes for mass spectrometry

mEmerald protein complex isolation mass spectrometry was performed as previously described [70], utilizing GFP-Trap magnetic beads (Chromotek). Briefly, U-2 OS cells expressing mEmerald constructs were washed twice with cold PBS (Thermo Fisher, #14190144), harvested by scraping with a cell lifter, and centrifuged at 350 g for 10 min at 4°C. Cell pellets were resuspended in 1 mL resuspension buffer (20mM HEPES, pH 7.4, 1.2% polyvinylpyrrolidone) with protease (MiliporeSigma, #8340) and phosphatase inhibitors (MiliporeSigma, #5726 and #P0044), and snap frozen in liquid nitrogen. Cells were lysed by cryogenic grinding using a MM 301 Mixer Mill (10 cycles, 2.5 min at 30Hz) (Retsch). Lysate was resuspended in MS lysis buffer (20 mM K-HEPES pH 7.4, 150 mM NaCl, 100 mM KOAc, 2 mM MgCl2, 0.1% Tween-20, 1 µm ZnCl2 1 µm CaCl2, 0.5% Triton X-100) with protease and phosphatase inhibitors (5 ml/g cells). Resuspended lysate was homogenized using a Polytron (Kinematica) (2 × 15 sec at 25,000 RPM) and pelleted at 2500 g at 4°C. Cleared lysate was incubated with 50 µl equilibrated GFP-Trap magnetic beads by rotating for 1 hr at 4°C. Beads were washed 6 times with 1 ml of lysis buffer. GFP complexes were eluted from beads in 40 µl 1X LDS Sample Buffer (Invitrogen) at 70°C for 15 min. Eluted complexes were alkylated with 100 mM iodoacetamide for 1 hr at room temperature prior to mass spectrometry analysis. Two independent biological replicates were analyzed in duplicate.

Liquid chromatography-tandem mass spectrometry (LC-MS/MS) analysis

Immunoprecipitated samples were subjected to SDS-PAGE and stained with coomassie. Lanes (1 cm) for each sample were excised and the proteins were reduced with 5 mM DTT for 30 min at 55°C, alkylated with 15 mM IAA for 45 min in the dark at room temperature, and in-gel digested with trypsin overnight at 37°C. Peptides were extracted, desalted with C18 spin columns (Pierce), and dried via vacuum centrifugation. Peptide samples were stored at −80°C until further analysis.

Each sample was analyzed in duplicate by LC-MS/MS using an Easy nLC 1200 coupled to a QExactive HF (Thermo Scientific). Samples were injected onto an Easy Spray PepMap C18 column (75 µm id × 25 cm, 2 µm particle size) (Thermo Scientific) and separated

over a 60 min method. The gradient for separation consisted of 5–45% mobile phase B at a 250 nl/min flow rate, where mobile phase A was 0.1% formic acid in water and mobile phase B consisted of 0.1% formic acid in 80% ACN. The QExactive HF was operated in data-dependent mode, where the 15 most intense precursors were selected for subsequent HCD fragmentation. Resolution for the precursor scan (m/z 350–1600) was set to 60,000, while MS/MS scans resolution was set to 15,000. The normalized collision energy was set to 27% for HCD. Peptide match was set to preferred, and precursors with unknown charge or a charge state of 1 and ≥ 7 were excluded.

Raw data files were processed using Proteome Discoverer version 2.1 (Thermo Scientific). Peak lists were searched against a reviewed Uniprot human database (containing 20,414 protein sequences, downloaded January 2019). appended with a common contaminants database. The following parameters were used to identify tryptic peptides for protein identification: 10 ppm precursor ion mass tolerance; 0.02 Da product ion mass tolerance; up to two missed trypsin cleavage sites; carbamidomethylation of Cys was set as a fixed modification; oxidation of was set as a variable modification. Scaffold (version 4.7.3, Proteome Software) was used to validate MS/MS-based peptide and protein identifications, and to provide relative quantitation. Peptide identifications were accepted if they could be established at greater than 95% probability to achieve an FDR less than 0.1% by the Scaffold Local FDR algorithm. Protein identifications were accepted if they could be established at greater than 99.0% probability and contained at least 2 identified peptides. SAINT (Significance Analysis of INTeractome) [39] was used to identify PLIN5 interactors. Proteins were identified as PLIN5 interactors if they had a FC_A (Average enrichment relative to Em control) score greater than 2.0 and a SAINT score greater than 0.75. Relative quantitation was performed using the calculated quantitative values (normalized peak areas) within Scaffold.

Isolation of GFP-PLIN5 complexes for co-immunoprecipitation/western blot

Isolation of mEmerald protein complexes for co-immunoprecipitation was performed utilizing the same harvesting method used for mass spectrometry. Following cell harvesting, Co-immunoprecipitation was performed utilizing GFP-Trap magnetic beads (Chromotek) following manufacturer protocols with slight modification. Cell pellets were resuspended in 400 µL of Co-IP Lysis Buffer (10 mM Tris/Cl pH 7.5; 150 mM NaCl; 0.5 mM EDTA; 0.5% NP-40) with protease and phosphatase inhibitors. The cell suspension was then incubated on ice for 30 min with pipetting every 10 minutes and then pelleted at 20,000 g for 10 min at 4 °C. 600 µl of Co-IP Dilution Buffer (10 mM Tris-Cl pH 7.5; 150 mM NaCl; 0.5 mM EDTA) was added to cleared lysate. Diluted lysate was incubated with 25 µl equilibrated GFP-Trap magnetic beads by rotating for 1 hr at 4 °C. Beads were washed 3 times with 500 ul of Co-IP Dilution Buffer. GFP complexes were eluted from beads in 30 µl 6X Laemmli Sample Buffer at 95 °C for 10 min. Protein complexes were examined by Western blotting.

Quantitative real-time PCR

RNA was isolated using RNeasy Plus Mini kit (Qiagen, 74134) per manufacturer's instructions. 1 µg of RNA was reverse transcribed to cDNA using the High-Capacity RNA-to-cDNA kit (Applied Biosystems, 4387406). cDNA was diluted

1:2, and 4 μL of each sample was amplified by real-time PCR using SYBR Green PCR Master Mix (Applied Biosystems, 4309155) in 20 μL total volume reactions on an Applied Biosystems' QuantStudio 7 Flex machine. Primers for PLIN5 (forward: 5'-CCATCTCGCCTATGAACACTCTT-3' and reverse: 5'-CAGCTGGGCCAGCATCTC-3') and 18S (forward: 5'-GTAACCCGTTGAACCCCATT-3' and reverse: 5'-CCATCCAATCGGTAGAGCG-3'), were used as previously described[37]. Expression was normalized to 18S as an endogenous control and qPCR data were analyzed using the comparative Ct method (2-ΔΔCt)[71].

Microscopy and image processing

Images were acquired on an inverted Zeiss 800/Airyscan laser scanning confocal microscope equipped with 405, 488, 561 and 647 nm diode lasers, and Galium Arsenide Phosphid (GaAsP) and Airyscan detectors. Confocal and Airyscan images were acquired using a 63x/1.4 NA objective lens, at 37 °C and 5% CO_2 (Carl Zeiss, Oberkochen, Germany). For movies S1–S4, Airyscan timelapse images were acquired every 27 s for 10 frames. Airyscan images were processed in Zen software (Carl Zeiss) using a processing strength of 6.0.

Image brightness and contrast were adjusted in Adobe Photoshop CS.

Quantification and statistical analysis

Images were analyzed using ImageJ (NIH)[72] and CellProfiler[73].

For organelle colocalization, masks of each organelle were created using the corresponding channels. For overlap of LDs with organelles (mitochondria, peroxisomes), the percentage of LD pixels colocalized with the organelle versus total LD pixels was calculated. For overlap of peroxisomes with mitochondria, the percentage of peroxisome pixels colocalized with the organelle versus total peroxisome pixels was calculated. For overlap of mitochondria with the ER, the percentage of mitochondria pixels colocalized with the ER versus total mitochondria pixels was calculated

LDs were tracked using the TrackMate[74] plugin, an ImageJ implementation of the linear assignment problem (LAP) tracking algorithm[75].

For fluorescent FA pulse-chase assays, images were analyzed using ImageJ to determine fluorescence intensity/cell. To quantify the fluorescence intensity of Red C12 in mitochondria and LDs, we made mitochondria and LD masks using the Mito-GFP and Bodipy 665/667 channels respectively, after which the fluorescence intensity in the Red C12 channel was calculated across the entire mask.

Statistical detail for all experiments can be found in the figure legends. Statistical analysis among groups was performed using Student's t test.

Supplementary Material

Refer to Web version on PubMed Central for supplementary material.

Acknowledgements

We thank Frank Conlon, Amit Joshi and current members of the Cohen lab for helpful discussions and critical reading of the manuscript. We are grateful to Reginald Edwards for performing pilot LD tracking experiments. This research is based in part upon work conducted using the UNC Proteomics Core Facility, which is supported in part by P30 CA016086 Cancer Center Core Support Grant to the UNC Lineberger Comprehensive Cancer Center. Research reported in this publication was supported by the National Institute of General Medical Sciences of the National Institutes of Health under award numbers R35 GM133460 (S.C.), F32 GM136027 (G.E.M.), R35 GM128666 (M.V.A.), and T32 GM135746 (D.W.G). Research reported in this publication was also supported by a Sloan Research Fellowship (M.V.A.)

Inclusion and Diversity

One or more of the authors of this paper self-identifies as an underrepresented ethnic minority in their field of research or within their geographical location. One or more of the authors of this paper self-identifies as a gender minority in their field of research. One or more of the authors of this paper received support from a program designed to increase minority representation in their field of research.

References

1. Prinz WA, Toulmay A, and Balla T (2019). The functional universe of membrane contact sites. Nat Rev Mol Cell Biol 21, 7–24. 10.1038/s41580-019-0180-9. [PubMed: 31732717]
2. Bohnert M (2020). Tether Me, Tether Me Not—Dynamic Organelle Contact Sites in Metabolic Rewiring. Dev Cell 54, 212–225. 10.1016/J.DEVCEL.2020.06.026. [PubMed: 32693056]
3. Zechner R, Madeo F, and Kratky D (2017). Cytosolic lipolysis and lipophagy: two sides of the same coin. Nat Rev Mol Cell Biol 18, 671–684. 10.1038/nrm.2017.76. [PubMed: 28852221]
4. Wang H, Sreenivasan U, Hu H, Saladino A, Polster BM, Lund LM, Gong D, Stanley WC, and Sztalryd C (2011). Perilipin 5, a lipid droplet-associated protein, provides physical and metabolic linkage to mitochondria. J Lipid Res 52, 2159. 10.1194/JLR.M017939. [PubMed: 21885430]
5. Daemen S, Van Polanen N, and Hesselink MKC (2018). The effect of diet and exercise on lipid droplet dynamics in human muscle tissue. J Exp Biol 221. 10.1242/JEB.167015.
6. Rambold AS, Cohen S, and Lippincott-Schwartz J (2015). Fatty Acid Trafficking in Starved Cells: Regulation by Lipid Droplet Lipolysis, Autophagy, and Mitochondrial Fusion Dynamics. Dev Cell 32, 678–692. 10.1016/J.DEVCEL.2015.01.029. [PubMed: 25752962]
7. Herms A, Bosch M, Reddy BJN, Schieber NL, Fajardo A, Rupérez C, Fernández-Vidal A, Ferguson C, Rentero C, Tebar F, et al. (2015). AMPK activation promotes lipid droplet dispersion on detyrosinated microtubules to increase mitochondrial fatty acid oxidation. Nature Communications 2015 6:1 6, 1–14. 10.1038/ncomms8176.
8. Nguyen TB, Louie SM, Daniele JR, Tran Q, Dillin A, Zoncu R, Nomura DK, and Olzmann JA (2017). DGAT1-dependent lipid droplet biogenesis protects mitochondrial function during starvation-induced autophagy. Dev Cell 42, 9. 10.1016/J.DEVCEL.2017.06.003. [PubMed: 28697336]
9. Valm AM, Cohen S, Legant WR, Melunis J, Hershberg U, Wait E, Cohen AR, Davidson MW, Betzig E, and Lippincott-Schwartz J (2017). Applying systems-level spectral imaging and analysis to reveal the organelle interactome. Nature 546, 162–167. 10.1038/nature22369. [PubMed: 28538724]
10. Benador IY, Veliova M, Mahdaviani K, Petcherski A, Wikstrom JD, Assali EA, Acín-Pérez R, Shum M, Oliveira MF, Cinti S, et al. (2018). Mitochondria Bound to Lipid Droplets Have Unique Bioenergetics, Composition, and Dynamics that Support Lipid Droplet Expansion. Cell Metab 27, 869–885.e6. [PubMed: 29617645]
11. Wang H, and Sztalryd C (2011). Oxidative tissue: perilipin 5 links storage with the furnace. Trends Endocrinol Metab 22, 197–203. 10.1016/j.tem.2011.03.008. [PubMed: 21632259]

12. Benador IY, Veliova M, Liesa M, and Shirihai OS (2019). Mitochondria Bound to Lipid Droplets: Where Mitochondrial Dynamics Regulate Lipid Storage and Utilization. Cell Metab 29, 827–835. 10.1016/J.CMET.2019.02.011. [PubMed: 30905670]

13. Schuldiner M, and Bohnert M (2017). A different kind of love – lipid droplet contact sites. Biochimica et Biophysica Acta (BBA) - Molecular and Cell Biology of Lipids 1862, 1188–1196. 10.1016/J.BBALIP.2017.06.005. [PubMed: 28627434]

14. Olzmann JA, and Carvalho P (2018). Dynamics and functions of lipid droplets. Nat Rev Mol Cell Biol 20, 137–155. 10.1038/s41580-018-0085-z.

15. Kimmel AR, and Sztalryd C (2016). The Perilipins: Major Cytosolic Lipid Droplet–Associated Proteins and Their Roles in Cellular Lipid Storage, Mobilization, and Systemic Homeostasis*. 10.1146/annurev-nutr-071813-10541036, 471–509. 10.1146/ANNUREV-NUTR-071813-105410.

16. Gemmink A, Daemen S, Kuijpers HJH, Schaart G, Duimel H, López-Iglesias C, van Zandvoort MAMJ, Knoops K, and Hesselink MKC (2018). Super-resolution microscopy localizes perilipin 5 at lipid droplet-mitochondria interaction sites and at lipid droplets juxtaposing to perilipin 2. Biochimica et Biophysica Acta (BBA) - Molecular and Cell Biology of Lipids 1863, 1423–1432. 10.1016/J.BBALIP.2018.08.016. [PubMed: 30591149]

17. Kuramoto K, Okamura T, Yamaguchi T, Nakamura TY, Wakabayashi S, Morinaga H, Nomura M, Yanase T, Otsu K, Usuda N, et al. (2012). Perilipin 5, a Lipid Droplet-binding Protein, Protects Heart from Oxidative Burden by Sequestering Fatty Acid from Excessive Oxidation. Journal of Biological Chemistry 287, 23852–23863. 10.1074/JBC.M111.328708. [PubMed: 22532565]

18. Mason RR, Mokhtar R, Matzaris M, Selathurai A, Kowalski GM, Mokbel N, Meikle PJ, Bruce CR, and Watt MJ (2014). PLIN5 deletion remodels intracellular lipid composition and causes insulin resistance in muscle. Mol Metab 3, 652–663. 10.1016/J.MOLMET.2014.06.002. [PubMed: 25161888]

19. Drevinge C, Dalen KT, Mannila MN, Täng MS, Ståhlman M, Klevstig M, Lundqvist A, Mardani I, Haugen F, Fogelstrand P, et al. (2016). Perilipin 5 is protective in the ischemic heart. Int J Cardiol 219, 446–454. 10.1016/J.IJCARD.2016.06.037. [PubMed: 27376234]

20. Zheng P, Xie Z, Yuan Y, Sui W, Wang C, Gao X, Zhao Y, Zhang F, Gu Y, Hu P, et al. (2017). Plin5 alleviates myocardial ischaemia/reperfusion injury by reducing oxidative stress through inhibiting the lipolysis of lipid droplets. 7. 10.1038/srep42574.

21. Wang H, Sreenivasan U, Gong DW, O'Connell KA, Dabkowski ER, Hecker PA, Ionica N, Konig M, Mahurkar A, Sun Y, et al. (2013). Cardiomyocyte-specific perilipin 5 overexpression leads to myocardial steatosis and modest cardiac dysfunction. J Lipid Res 54, 953–965. 10.1194/JLR.M032466. [PubMed: 23345411]

22. Montgomery MK, Watt MJ, Keenan SN, Meex RC, Lo JCY, Ryan A, and Nie S (2019). Perilipin 5 Deletion in Hepatocytes Remodels Lipid Metabolism and Causes Hepatic Insulin Resistance in Mice. Diabetes 68, 543–555. 10.2337/DB18-0670. [PubMed: 30617219]

23. Bosma M, Sparks LM, Hooiveld GJ, Jorgensen JA, Houten SM, Schrauwen P, Kersten S, and Hesselink MKC (2013). Overexpression of PLIN5 in skeletal muscle promotes oxidative gene expression and intramyocellular lipid content without compromising insulin sensitivity. Biochimica et Biophysica Acta (BBA) - Molecular and Cell Biology of Lipids 1831, 844–852. 10.1016/J.BBALIP.2013.01.007. [PubMed: 23353597]

24. Gallardo-Montejano VI, Yang C, Hahner L, McAfee JL, Johnson JA, Holland WL, Fernandez-Valdivia R, and Bickel PE (2021). Perilipin 5 links mitochondrial uncoupled respiration in brown fat to healthy white fat remodeling and systemic glucose tolerance. Nature Communications 2021 12:1 12, 1–18. 10.1038/s41467-021-23601-2.

25. Pollak NM, Jaeger D, Kolleritsch S, Zimmermann R, Zechner R, Lass A, and Haemmerle G (2015). The interplay of protein kinase A and perilipin 5 regulates cardiac lipolysis. J Biol Chem 290, 1295–1306. 10.1074/jbc.M114.604744. [PubMed: 25418045]

26. Keenan SN, Nardo W. de, Lou J, Schittenhelm RB, Montgomery MK, Granneman JG, Hinde E, and Watt MJ (2021). Perilipin 5 S155 phosphorylation by PKA is required for the control of hepatic lipid metabolism and glycemic control. J Lipid Res 62. 10.1194/JLR.RA120001126.

27. Herrmann T, Buchkremer F, Gosch I, Hall AM, Bernlohr DA, and Stremmel W (2001). Mouse fatty acid transport protein 4 (FATP4): Characterization of the gene and functional assessment

as a very long chain acyl-CoA synthetase. Gene 270, 31–40. 10.1016/S0378-1119(01)00489-9. [PubMed: 11404000]

28. Roy A, Kucukural A, and Zhang Y (2010). I-TASSER: a unified platform for automated protein structure and function prediction. Nature Protocols 2010 5:4 5, 725–738. 10.1038/nprot.2010.5.
29. Yang J, Yan R, Roy A, Xu D, Poisson J, and Zhang Y (2015). The I-TASSER Suite: protein structure and function prediction. Nat Methods 12, 7–8. 10.1038/nmeth.3213.
30. Yang J, and Zhang Y (2015). I-TASSER server: new development for protein structure and function predictions. Nucleic Acids Res 43, W174. 10.1093/NAR/GKV342. [PubMed: 25883148]
31. Xu D, and Zhang Y (2012). Ab initio protein structure assembly using continuous structure fragments and optimized knowledge-based force field. Proteins: Structure, Function, and Bioinformatics 80, 1715–1735. 10.1002/PROT.24065.
32. Xu D, and Zhang Y (2013). Toward optimal fragment generations for ab initio protein structure assembly. Proteins: Structure, Function, and Bioinformatics 81, 229–239. 10.1002/PROT.24179.
33. Najt CP, Khan SA, Heden TD, Witthuhn BA, Perez M, Heier JL, Mead LE, Franklin MP, Karanja KK, Graham MJ, et al. (2020). Lipid Droplet-Derived Monounsaturated Fatty Acids Traffic via PLIN5 to Allosterically Activate SIRT1. Mol Cell 77, 810–824.e8. 10.1016/J.MOLCEL.2019.12.003. [PubMed: 31901447]
34. Wang H, Becuwe M, Housden BE, Chitraju C, Porras AJ, Graham MM, Liu XN, Thiam AR, Savage DB, Agarwal AK, et al. (2016). Seipin is required for converting nascent to mature lipid droplets. Elife 5. 10.7554/ELIFE.16582.
35. Kilwein MD, and Welte MA (2019). Lipid Droplet Motility and Organelle Contacts. Contact 2, 251525641989568. 10.1177/2515256419895688.
36. Wang H, Bell M, Sreenevasan U, Hu H, Liu J, Dalen K, Londos C, Yamaguchi T, Rizzo MA, Coleman R, et al. (2011). Unique Regulation of Adipose Triglyceride Lipase (ATGL) by Perilipin 5, a Lipid Droplet-associated Protein. J Biol Chem 286, 15707. 10.1074/JBC.M110.207779. [PubMed: 21393244]
37. Gallardo-Montejano VI, Saxena G, Kusminski CM, Yang C, McAfee JL, Hahner L, Hoch K, Dubinsky W, Narkar VA, and Bickel PE (2016). Nuclear Perilipin 5 integrates lipid droplet lipolysis with PGC-1α/SIRT1-dependent transcriptional regulation of mitochondrial function. Nat Commun 7, 12723. 10.1038/ncomms12723. [PubMed: 27554864]
38. Kannan M, Lahiri S, Liu LK, Choudhary V, and Prinz WA (2017). Phosphatidylserine synthesis at membrane contact sites promotes its transport out of the ER. J Lipid Res 58, 553–562. 10.1194/JLR.M072959. [PubMed: 28119445]
39. Choi H, Liu G, Mellacheruvu D, Tyers M, Gingras AC, and Nesvizhskii AI (2012). Analyzing protein-protein interactions from affinity purification-mass spectrometry data with SAINT. Current protocols in bioinformatics / editoral board, Andreas D. Baxevanis … [et al.] CHAPTER, Unit8.15. 10.1002/0471250953.BI0815S39.
40. Steensels S, Qiao J, Zhang Y, Maner-Smith KM, Kika N, Holman CD, Corey KE, Bracken WC, Ortlund EA, and Ersoy BA (2020). Acyl-Coenzyme A Thioesterase 9 Traffics Mitochondrial Short-Chain Fatty Acids Toward De Novo Lipogenesis and Glucose Production in the Liver. Hepatology 72, 857–872. 10.1002/HEP.31409. [PubMed: 32498134]
41. Hall AM, Wiczer BM, Herrmann T, Stremmel W, and Bernlohr DA (2005). Enzymatic Properties of Purified Murine Fatty Acid Transport Protein 4 and Analysis of Acyl-CoA Synthetase Activities in Tissues from FATP4 Null Mice *. Journal of Biological Chemistry 280, 11948–11954. 10.1074/JBC.M412629200. [PubMed: 15653672]
42. Lobo S, Wiczer BM, Smith AJ, Hall AM, and Bernlohr DA (2007). Fatty acid metabolism in adipocytes: functional analysis of fatty acid transport proteins 1 and 4. J Lipid Res 48, 609–620. 10.1194/JLR.M600441-JLR200. [PubMed: 17164224]
43. Jia Z, Moulson CL, Pei Z, Miner JH, and Watkins PA (2007). Fatty Acid Transport Protein 4 Is the Principal Very Long Chain Fatty Acyl-CoA Synthetase in Skin Fibroblasts. Journal of Biological Chemistry 282, 20573–20583. 10.1074/JBC.M700568200. [PubMed: 17522045]
44. Jia Z, Pei Z, Maiguel D, Toomer CJ, and Watkins PA (2007). The fatty acid transport protein (FATP) family: Very long chain acyl-CoA synthetases or solute carriers? Journal of Molecular Neuroscience 33, 25–31. 10.1007/S12031-007-0038-Z/FIGURES/6. [PubMed: 17901542]

45. Young PA, Senkal CE, Suchanek AL, Grevengoed TJ, Lin DD, Zhao L, Crunk AE, Klett EL, Füllekrug J, Obeid LM, et al. (2018). Long-chain acyl-CoA synthetase 1 interacts with key proteins that activate and direct fatty acids into niche hepatic pathways. Journal of Biological Chemistry 293, 16724–16740. 10.1074/JBC.RA118.004049. [PubMed: 30190326]
46. Shepherd SO, Cocks M, Tipton KD, Ranasinghe AM, Barker TA, Burniston JG, Wagenmakers AJM, and Shaw CS (2013). Sprint interval and traditional endurance training increase net intramuscular triglyceride breakdown and expression of perilipin 2 and 5. J Physiol 591, 657. 10.1113/JPHYSIOL.2012.240952. [PubMed: 23129790]
47. Jeppesen J, Jordy AB, Sjøberg KA, Füllekrug J, Stahl A, Nybo L, and Kiens B (2012). Enhanced Fatty Acid Oxidation and FATP4 Protein Expression after Endurance Exercise Training in Human Skeletal Muscle. PLoS One 7, e29391. 10.1371/JOURNAL.PONE.0029391. [PubMed: 22235293]
48. Tarnopolsky MA, Rennie CD, Robertshaw HA, Fedak-Tarnopolsky SN, Devries MC, and Hamadeh MJ (2007). Influence of endurance exercise training and sex on intramyocellular lipid and mitochondrial ultrastructure, substrate use, and mitochondrial enzyme activity. Am J Physiol Regul Integr Comp Physiol 292, 1271–1278. 10.1152/AJPREGU.00472.2006/ASSET/IMAGES/LARGE/ZH60030756800003.JPEG.
49. Devries MC, Samjoo IA, Hamadeh MJ, McCready C, Raha S, Watt MJ, Steinberg GR, and Tarnopolsky MA (2013). Endurance Training Modulates Intramyocellular Lipid Compartmentalization and Morphology in Skeletal Muscle of Lean and Obese Women. J Clin Endocrinol Metab 98, 4852–4862. 10.1210/JC.2013-2044. [PubMed: 24081737]
50. Boutant M, Kulkarni SS, Joffraud M, Ratajczak J, Valera-Alberni M, Combe R, Zorzano A, and Cantó C (2017). Mfn2 is critical for brown adipose tissue thermogenic function. EMBO J 36, 1543–1558. 10.15252/EMBJ.201694914. [PubMed: 28348166]
51. Cho KF, Branon TC, Rajeev S, Svinkina T, Udeshi ND, Thoudam T, Kwak C, Rhee H-W, Lee I-K, Carr SA, et al. (2020). Split-TurboID enables contact-dependent proximity labeling in cells. Proceedings of the National Academy of Sciences 117, 12143–12154. 10.1073/PNAS.1919528117.
52. Prinz WA (2014). Bridging the gap: membrane contact sites in signaling, metabolism, and organelle dynamics. J Cell Biol 205, 759–769. 10.1083/jcb.201401126. [PubMed: 24958771]
53. MacPherson REK, Ramos SV, Vandenboom R, Roy BD, and Peters SJ (2013). Skeletal muscle PLIN proteins, ATGL and CGI-58, interactions at rest and following stimulated contraction. Am J Physiol Regul Integr Comp Physiol 304, R644. 10.1152/AJPREGU.00418.2012. [PubMed: 23408028]
54. Huh JY, Reilly SM, Abu-Odeh M, Murphy AN, Mahata SK, Zhang J, Cho Y, Seo JB, Hung CW, Green CR, et al. (2020). TANK-Binding Kinase 1 Regulates the Localization of Acyl-CoA Synthetase ACSL1 to Control Hepatic Fatty Acid Oxidation. Cell Metab 32, 1012–1027.e7. 10.1016/J.CMET.2020.10.010. [PubMed: 33152322]
55. Datta S, Bowerman J, Hariri H, Ugrankar R, Eckert KM, Corley C, Vale G, McDonald JG, and Mike Henne W (2020). Snx14 proximity labeling reveals a role in saturated fatty acid metabolism and ER homeostasis defective in SCAR20 disease. Proc Natl Acad Sci U S A 117, 33282–33294. 10.1073/PNAS.2011124117/-/DCSUPPLEMENTAL. [PubMed: 33310904]
56. Küch EM, Vellaramkalayil R, Zhang I, Lehnen D, Brügger B, Stremmel W, Ehehalt R, Poppelreuther M, and Füllekrug J (2014). Differentially localized acyl-CoA synthetase 4 isoenzymes mediate the metabolic channeling of fatty acids towards phosphatidylinositol. Biochimica et Biophysica Acta (BBA) - Molecular and Cell Biology of Lipids 1841, 227–239. 10.1016/J.BBALIP.2013.10.018. [PubMed: 24201376]
57. Kassan A, Herms A, Fernández-Vidal A, Bosch M, Schieber NL, Reddy BJN, Fajardo A, Gelabert-Baldrich M, Tebar F, Enrich C, et al. (2013). Acyl-CoA synthetase 3 promotes lipid droplet biogenesis in ER microdomains. Journal of Cell Biology 203, 985–1001. 10.1083/JCB.201305142/VIDEO-5. [PubMed: 24368806]
58. Kien B, Kolleritsch S, Kunowska N, Heier C, Chalhoub G, Tilp A, Wolinski H, Stelzl U, and Haemmerle G (2022). Lipid droplet-mitochondria coupling via Perilipin 5 augments respiratory capacity but is dispensable for FA oxidation. J Lipid Res, 100172. 10.1016/J.JLR.2022.100172. [PubMed: 35065923]

59. Ouyang Q, Chen Q, Ke S, Ding L, Yang X, Rong P, Feng W, Cao Y, Wang Q, Li M, et al. (2023). Rab8a as a mitochondrial receptor for lipid droplets in skeletal muscle. Dev Cell 58, 289–305. 10.1016/j.devcel.2023.01.007. [PubMed: 36800997]
60. Jägerström S, Polesie S, Wickström Y, Johansson BR, Schröder HD, Højlund K, and Boström P (2009). Lipid droplets interact with mitochondria using SNAP23. Cell Biol Int 33, 934–940. 10.1016/J.CELLBI.2009.06.011. [PubMed: 19524684]
61. Freyre CAC, Rauher PC, Ejsing CS, and Klemm RW (2019). MIGA2 Links Mitochondria, the ER, and Lipid Droplets and Promotes De Novo Lipogenesis in Adipocytes. Mol Cell 76, 811–825.e14. 10.1016/J.MOLCEL.2019.09.011. [PubMed: 31628041]
62. Wang J, Fang N, Xiong J, Du Y, Cao Y, and Ji WK (2021). An ESCRT-dependent step in fatty acid transfer from lipid droplets to mitochondria through VPS13D−TSG101 interactions. Nature Communications 2021 12:1 12, 1–16. 10.1038/s41467-021-21525-5.
63. Cui W, Sathyanarayan A, Lopresti M, Aghajan M, Chen C, and Mashek DG (2020). Lipophagy-derived fatty acids undergo extracellular efflux via lysosomal exocytosis. 10.1080/15548627.2020.172809717, 690–705. 10.1080/15548627.2020.1728097.
64. Perez-Riverol Y, Bai J, Bandla C, García-Seisdedos D, Hewapathirana S, Kamatchinathan S, Kundu DJ, Prakash A, Frericks-Zipper A, Eisenacher M, et al. (2022). The PRIDE database resources in 2022: a hub for mass spectrometry-based proteomics evidences. Nucleic Acids Res 50, D543–D552. 10.1093/NAR/GKAB1038. [PubMed: 34723319]
65. Mitra K, Wunder C, Roysam B, Lin G, and Lippincott-Schwartz J (2009). A hyperfused mitochondrial state achieved at G1-S regulates cyclin E buildup and entry into S phase. Proc Natl Acad Sci U S A 106, 11960–11965. 10.1073/PNAS.0904875106/SUPPL_FILE/SV5.MOV. [PubMed: 19617534]
66. Rambold AS, Kostelecky B, Elia N, and Lippincott-Schwartz J (2011). Tubular network formation protects mitochondria from autophagosomal degradation during nutrient starvation. Proc Natl Acad Sci U S A 108, 10190–10195. 10.1073/PNAS.1107402108/SUPPL_FILE/PNAS.201107402SI.PDF. [PubMed: 21646527]
67. Nixon-Abell J, Obara CJ, Weigel A. v., Li D, Legant WR, Xu CS, Pasolli HA, Harvey K, Hess HF, Betzig E, et al. (2016). Increased spatiotemporal resolution reveals highly dynamic dense tubular matrices in the peripheral ER. Science (1979) 354. 10.1126/SCIENCE.AAF3928/SUPPL_FILE/NIXON-ABELL.SM.PDF.
68. Friedman JR, Lackner LL, West M, DiBenedetto JR, Nunnari J, and Voeltz GK (2011). ER tubules mark sites of mitochondrial division. Science (1979) 334, 358–362. 10.1126/SCIENCE.1207385/SUPPL_FILE/FRIEDMAN.SOM.REV1.PDF.
69. Rys JP, DuFort CC, Monteiro DA, Baird MA, Oses-Prieto JA, Chand S, Burlingame AL, Davidson MW, and Alliston TN (2015). Discrete spatial organization of TGFβ receptors couples receptor multimerization and signaling to cellular tension. Elife 4. 10.7554/ELIFE.09300.
70. Kaltenbrun E, Greco TM, Slagle CE, Kennedy LM, Li T, Cristea IM, and Conlon FL (2013). A Gro/TLE-NuRD corepressor complex facilitates Tbx20-dependent transcriptional repression. J Proteome Res 12, 5395–5409. 10.1021/PR400818C. [PubMed: 24024827]
71. Livak KJ, and Schmittgen TD (2001). Analysis of Relative Gene Expression Data Using Real-Time Quantitative PCR and the 2−ΔΔCT Method. Methods 25, 402–408. 10.1006/METH.2001.1262. [PubMed: 11846609]
72. Schneider CA, Rasband WS, and Eliceiri KW (2012). NIH Image to ImageJ: 25 years of image analysis. Nature Methods 2012 9:7 9, 671–675. 10.1038/nmeth.2089.
73. Stirling DR, Swain-Bowden MJ, Lucas AM, Carpenter AE, Cimini BA, and Goodman A (2021). CellProfiler 4: improvements in speed, utility and usability. BMC Bioinformatics 22, 1–11. 10.1186/S12859-021-04344-9/FIGURES/6. [PubMed: 33388027]
74. Tinevez JY, Perry N, Schindelin J, Hoopes GM, Reynolds GD, Laplantine E, Bednarek SY, Shorte SL, and Eliceiri KW (2017). TrackMate: An open and extensible platform for single-particle tracking. Methods 115, 80–90. 10.1016/J.YMETH.2016.09.016. [PubMed: 27713081]
75. Jaqaman K, Loerke D, Mettlen M, Kuwata H, Grinstein S, Schmid SL, and Danuser G (2008). Robust single-particle tracking in live-cell time-lapse sequences. Nat Methods 5, 695–702. 10.1038/NMETH.1237. [PubMed: 18641657]

Highlights

- PLIN5 promotes lipid droplet (LD)-to-mitochondria fatty acid transport.
- This transport depends on PLIN5 phosphorylation and the PLIN5 C-terminal domain.
- The PLIN5 C-terminal domain interacts with FATP4 at membrane contact sites.
- FATP4 is required for mitochondrial fatty acid transport in starved myoblasts.

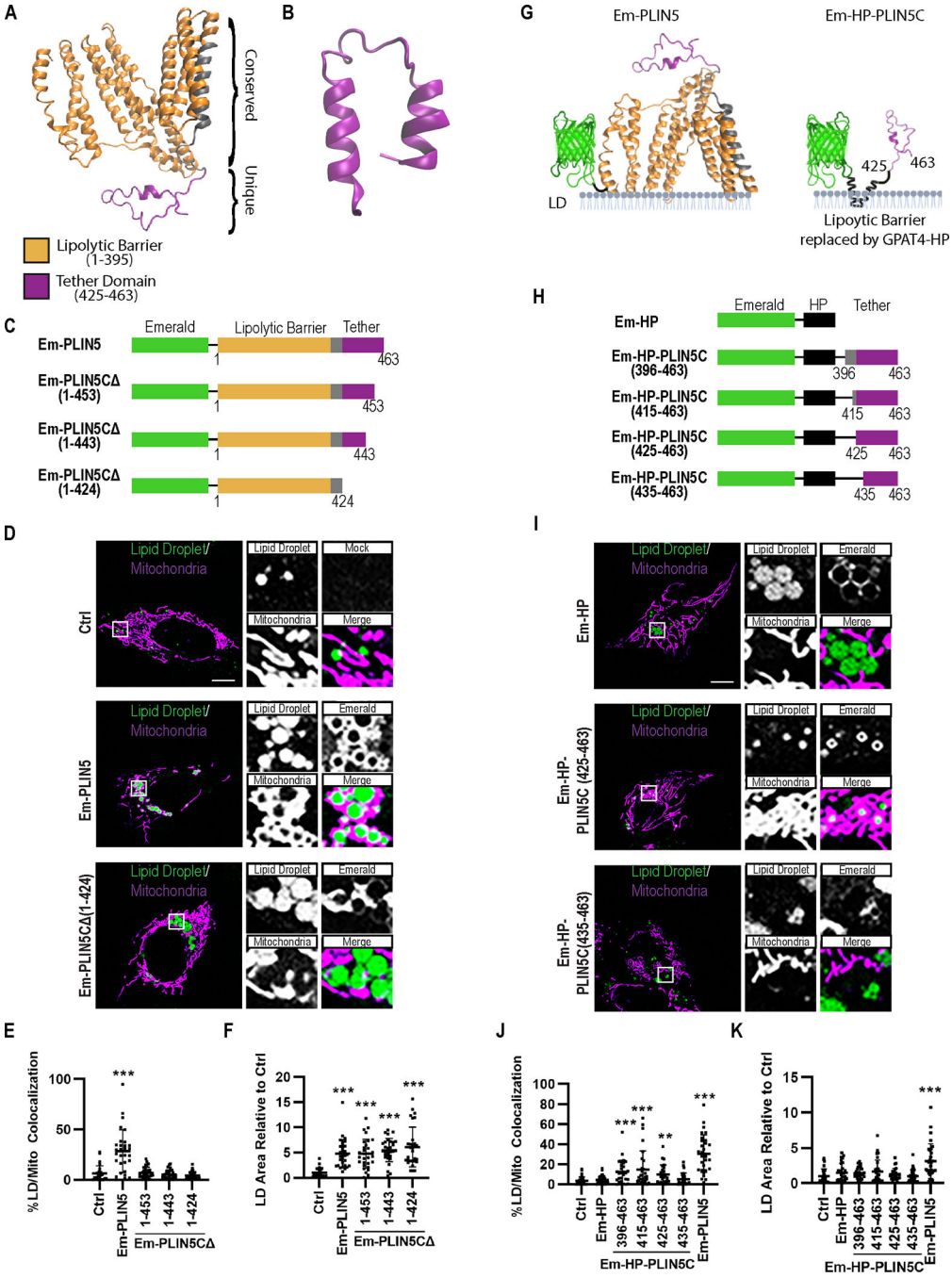

Figure 1. PLIN5 contains a C-terminal domain sufficient to promote LD-mito contacts

(A-B) Structure predictions of PLIN5. (A) I-TASSER structure prediction for PLIN5 showing the conserved perilipin lipolytic barrier domain (orange) and a putative C-terminal tether domain with no strong structural prediction (purple). (B) QUARK *de-novo* structure prediction for the putative tether domain shows a two alpha-helix structure containing a hydrophobic pocket. Schematic of mEmerald-tagged full-length PLIN5 and C-terminal truncations.

(C) Single focal plane micrographs of U-2 OS cells transfected with Mito-RFP and the indicated Em-PLIN5 construct, and labeled for LDs with Bodipy 665/676. Merged micrograph includes Mito-RFP and Bodipy 665/667 channels to demonstrate co-localization (white).

(E-F) Quantification of images from (D). (E) Colocalization of LDs with mitochondria was measured as % LD pixels overlapping with mitochondria, and (F) LD area/cell was measured, normalized to control. At least 27 cells were analyzed per condition across N=3 biological replicates.

(G-H) Design of constructs to target the C-terminal region of PLIN5 to the LD surface using the hairpin (HP) domain of Gpat4. (G) Cartoon depiction of constructs used to target PLIN5 C-terminal region to LD surface. Cartoon created with Biorender.com. (H) Schematic of mEmerald-tagged HP-PLIN5 constructs.

(I) Single focal plane micrographs of U-2 OS cells transfected with Mito-RFP and the indicated Em-PLIN5 construct, and labeled for LDs with Bodipy 665/676. Merged micrograph includes Mito-RFP and Bodipy 665/667 channels to demonstrate co-localization (white).

(J-K) Quantification of images from (I). (J) Colocalization of LDs with mitochondria was measured as % LD pixels overlapping with mitochondria, and (K) LD area/cell was measured, normalized to control. At least 26 cells were analyzed per condition across N=3 biological replicates.

Scale bar, 10μm. Error bars represent ± SD. **p < 0.01, ***p < 0.001.

See also Figure S1 and Supplemental Movies 1–4

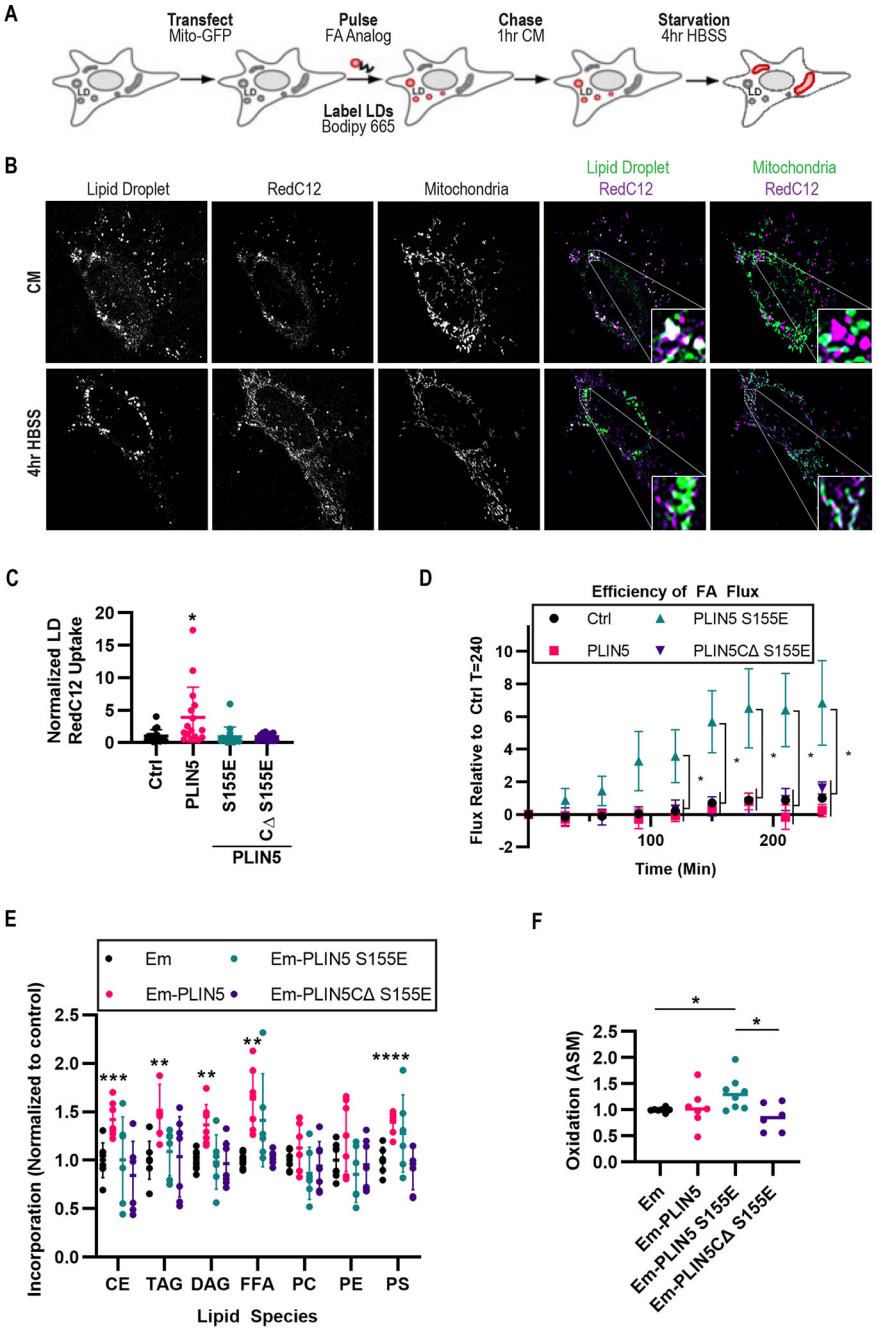

Figure 2. PLIN5 phosphorylation and LD-mito contacts drive ß-oxidation by increasing LD-to-mitochondria FA trafficking

(A) Schematic representation of FA analog pulse-chase assay design: C2C12 myoblasts were pulsed with FA analog overnight to allow accumulation into LDs and subsequently washed and chased with complete media (CM) for 1 hr. Following chase, incorporation of FA analog into LDs was measured. Cells were then incubated in HBSS for 4 or 6 hrs. and FA subcellular localization or oxidation was measured.

(B-D) Fluorescent pulse-chase assay. Control C2C12 myoblasts or C2C12 myoblasts overexpressing the indicated PLIN5 constructs were pulsed with Red C12 using the assay described in (A) to monitor FA trafficking from LDs to mitochondria. Following CM chase, cells were imaged to measure incorporation of Red C12 into LDs. Cells were then incubated in HBSS and imaged every 30 min for 4 hrs to monitor FA localization. (B) Representative single focal plane images of control cells following CM chase or 4 hr HBSS incubation. (C) Red C12 incorporation into LDs following CM chase measurements, normalized to control cells. At least 10 cells were analyzed per condition across N ≥ 3 biological replicates. Error bars represent ± SD. (D) Red C12 accumulation into mitochondria relative to initial LD incorporation following HBSS starvation, normalized to control cells. At least 10 cells were analyzed per condition across N ≥ 3 biological replicates. Data are expressed as means, error bars represent ± SEM.

(E-F) Radioactive pulse-chase assay. Control C2C12 myoblasts or C2C12 myoblasts overexpressing the indicated Em-PLIN5 constructs were pulsed with a radioactive FA analog [1-^{14}C]oleate using the assay described in (A) to monitor FA β-oxidation. Following media chase cells were either collected for TLC to measure incorporation of [1-^{14}C]oleate into cellular lipids or incubated in HBSS for 6 hrs to measure β-oxidation. (E) [1-^{14}C]oleate incorporation into lipid species following CM chase was measured by TLC and normalized to control cells. Lipid species abbreviations: Cholesterol Ester (CE), Triacylglycerol (TAG), Diacylglycerol (DAG), Free Fatty Acid (FFA), Phosphatidylcholine (PC), Phosphatidylethanolamine (PE), and Phosphatidylserine (PS). (F) β-oxidation following 6 hr incubation in HBSS was assessed by measuring ASM released into media relative to [1-^{14}C]oleate incorporation, normalized to control cells. N=4 biological replicates for all conditions. Error bars represent ± SD. Scale bar, 10 μm. *p < 0.05, **p < 0.01, ***p < 0.001 ****p < 0.0001. See also Figure S2

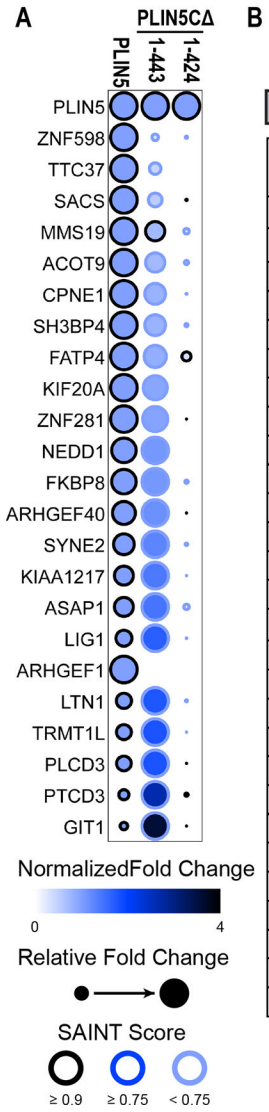

B

Mitochondrial

Protein Name	Fold Change (vs WT)	
	1-443	1-424
PLIN5	1.00	1.00
Fatty Acid Modifying		
FATP4	0.833	0.343
ACOT9	0.715	0.152
Transcription		
TASOR	1.100	0.026
MMS19	0.715	0.205
KIF20A	0.898	0.000
ZNF598	0.235	0.07
LIG1	1.660	0.036
SYNE2	1.287	0.118
PTCD3	2.617	0.326
TRMT1L	1.782	0.015
Membrane Trafficking		
ARHGEF1	1.682	0.061
SH3BP4	0.783	0.112
ARHGEF40	1.157	0.016
CPNE1	0.775	0.044
FKBP8	1.093	0.126
GIT1	3.559	0.032
ASAP1	1.417	0.282
Miscellaneous		
TTC37	0.434	0.005
LTN1	1.754	0.115
SACS	0.507	0.461
PLCD3	1.808	0.108
NEDD1	1.092	0.000
KIAA1217	1.407	0.040

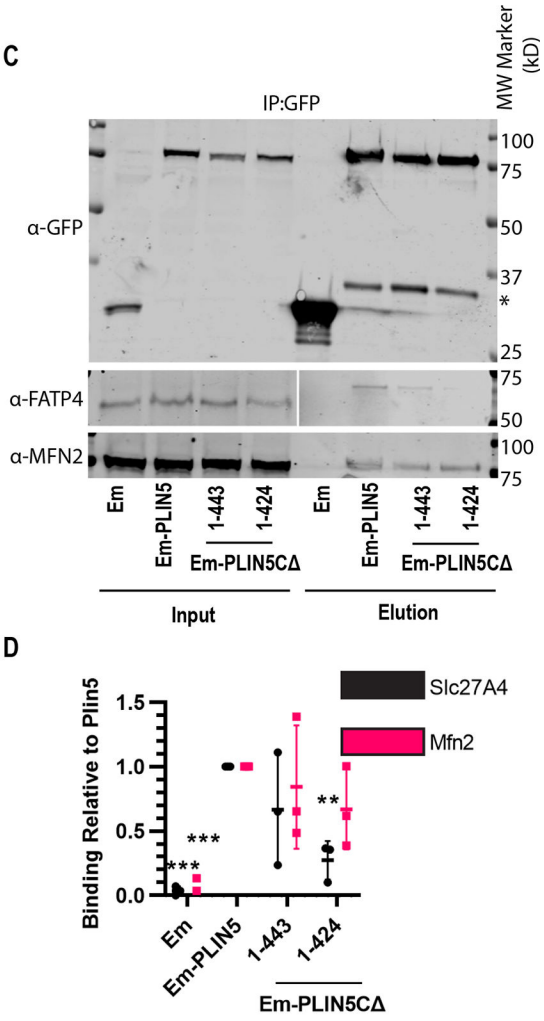

Figure 3. The PLIN5 tether domain interacts with acyl-CoA synthetase FATP4

(A-D) PLIN5 protein complexes were affinity purified from U-2 OS cells transfected with the indicated Em-PLIN5 construct and analyzed by mass spectrometry. (A) Graphical representation of PLIN5-associated protein complexes which show decreased abundance in PLIN5CΔ affinity purifications. Circle size and color represent relative enrichment, border color represents statistical significance. (B) Calculated fold change for each PLIN5-associated protein and proposed function. Proteins highlighted in grey show mitochondrial subcellular localization. (C) Western blot and (D) quantification of Mfn2 and FATP4 abundance in affinity-purified PLIN5 protein complexes. Protein abundance is relative to PLIN5, normalized to WT-PLIN5 affinity purification. * Indicates Em-PLIN5 degradation product. N = 3 biological replicates for each condition. Error bars represent ± SD. *p < 0.05, **p < 0.01, ***p < 0.001.

See also Supplemental Table 1

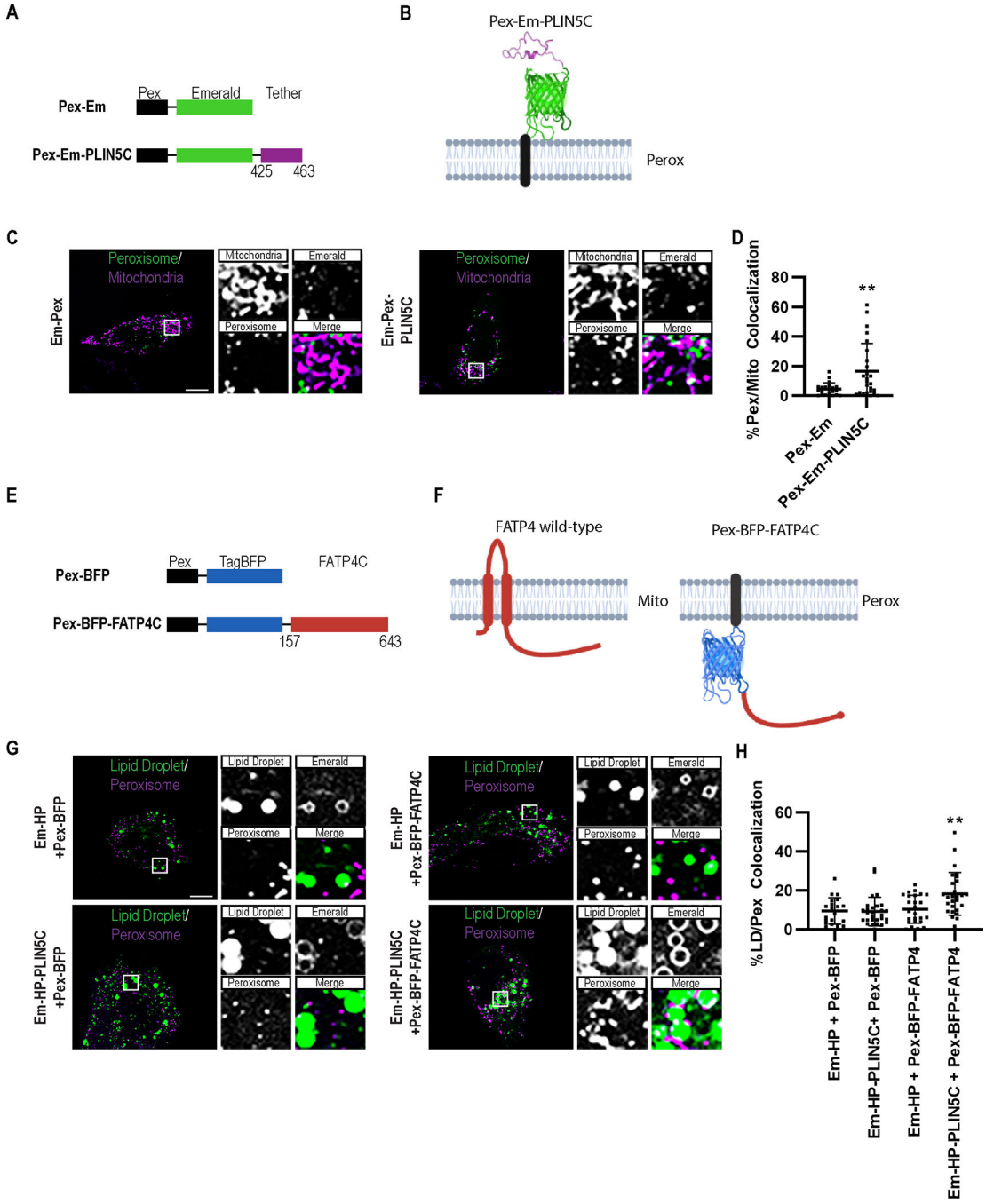

Figure 4. PLIN5 and FATP4 drive ectopic membrane contact sites

(A-B) Design of constructs targeting the tether domain of PLIN5 to the cytosolic face of the peroxisome membrane using the membrane-targeting sequence of Pex3 (Pex). (A) Schematic of mEmerald-tagged Pex constructs. (B) Cartoon depiction of construct used to target PLIN5 tether domain to peroxisome membrane. Cartoon created with Biorender.com. **(C)** Single focal plane micrographs of U-2 OS cells transfected with mOrange-SKL and the indicated Pex construct, mitochondria labeled with MitoTracker Deep Red FM. Merged

micrograph includes mOrange-SKL and MitoTracker Deep Red FM channels to demonstrate co-localization (white).

(D) Quantification of images from (C). Colocalization of peroxisomes with mitochondria was measured as % peroxisome pixels overlapping with mitochondria. At least 21 cells were analyzed per condition across N= 3 biological replicates.

(E-F) Design of constructs targeting the cytosolic domain of FATP4 to the cytosolic face of the peroxisome membrane using Pex. (E) Schematic of TagBFP-tagged Pex constructs. (F) Cartoon depiction of construct used to target FATP4 cytoplasmic domain to peroxisome membrane.

(G) Single focal plane micrographs of U-2 OS cells transfected with mOrange-SKL and the indicated HP/Pex targeted constructs, LDs labeled with Bodipy 665/676. Merged micrograph includes mOrange-SKL and Bodipy 665/676 channels to demonstrate co-localization (white).

(H) Quantification of images from (G). Colocalization of LDs with peroxisomes was measured as % LD pixels overlapping with peroxisomes. At least 20 cells were analyzed per condition across N= 3 biological replicates.

Scale bar, 10 μm. Error bars represent ± SD. **p < 0.01.

See also Figure S3

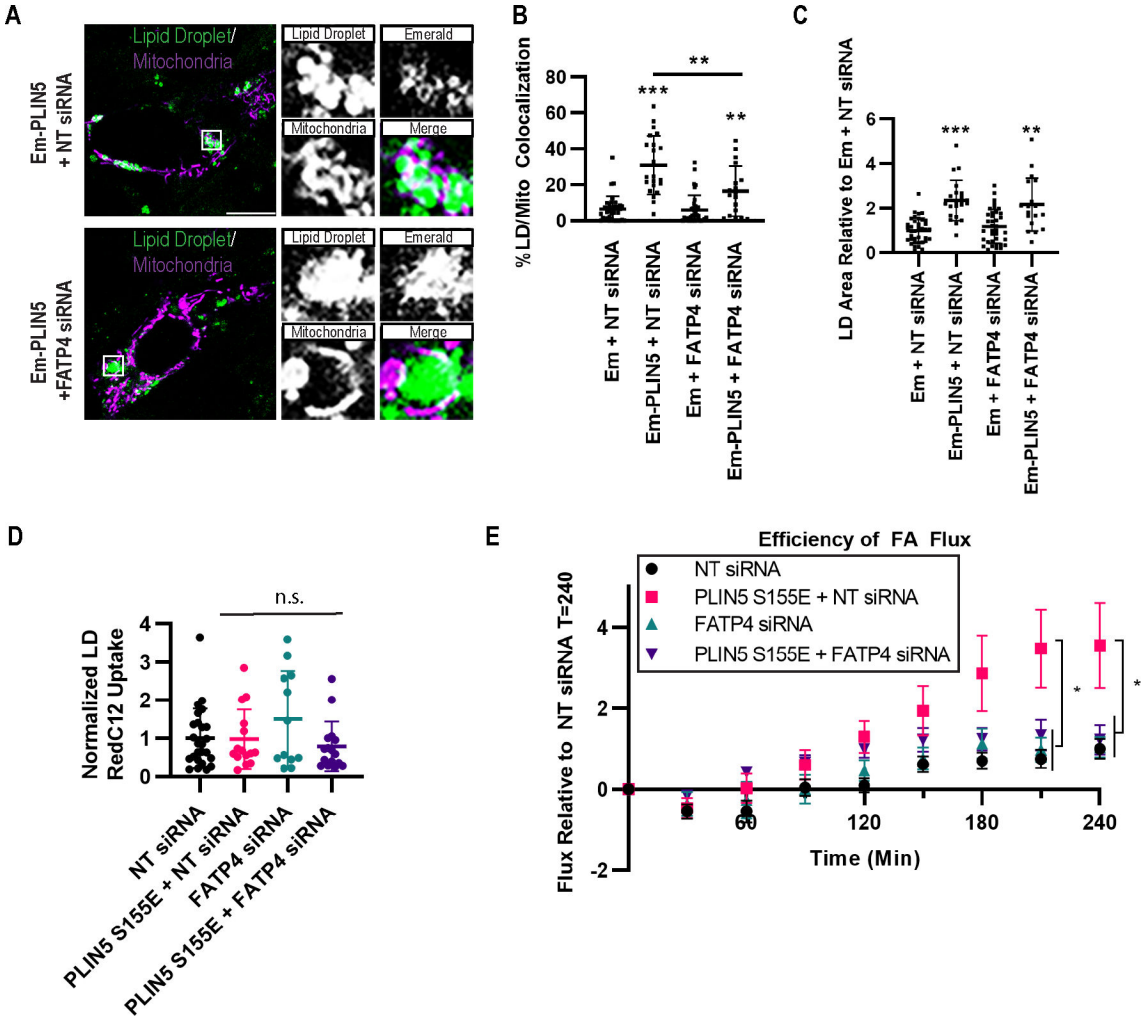

Figure 5. Loss of FATP4 impairs PLIN5-induced LD-mito contacts and FA trafficking

(A) Single focal plane micrographs of C2C12 myoblasts transfected for 24 hr with non-targeting or FATP4 siRNA. Following RNAi, cells were transfected with Mito-RFP and the indicated Em-PLIN5 construct, and LDs labeled with Bodipy 665/676. Merged micrograph includes Mito-RFP and Bodipy 665/676 channels to demonstrate co-localization (white).

(B-C) Quantification of images from A. (B) Colocalization of LDs with mitochondria was measured as % LD pixels overlapping with mitochondria, and (C) LD area/cell was measured, normalized to control. At least 18 cells were analyzed per condition across N ≥ 3 biological replicates. Error bars represent ± SD.

(D-E) C2C12 were assayed as described in Fig. 2A–B, following RNAi treatment using non-targeting or FATP4 siRNA. (D) Red C12 incorporation into LDs following CM chase was measured, normalized to control cells. Error bars represent ± SD. (E) Red C12 accumulation into mitochondria relative to initial LD incorporation following HBSS starvation was measured, normalized to control cells. At least 12 cells were analyzed per condition across N ≥ 3 biological replicates. Data are expressed as means, error bars represent ± SEM. Scale bar, 10 μm. *p < 0.05. **p < 0.01***p < 0.001.

See also Figure S4

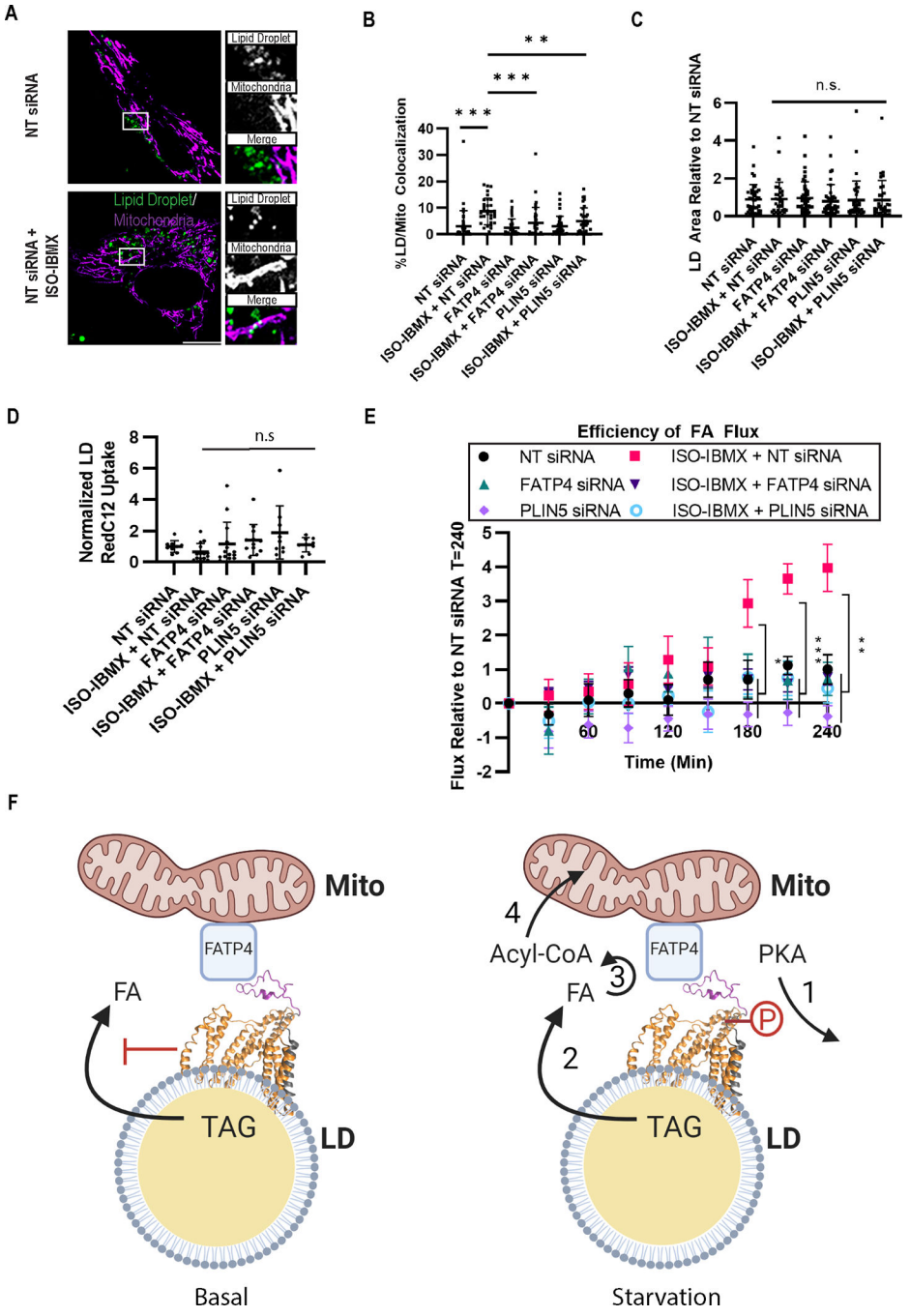

Figure 6. Endogenous PLIN5 and FATP4 induce LD-mito contacts and FA transfer in response to β-adrenergic signaling

(A) Single focal plane micrographs of C2C12 myoblasts transfected for 24 hr with non-targeting siRNA. Following RNAi, cells were transfected with Mito-RFP and LDs labeled with Bodipy 665/676. Cells were then treated with ISO-IBMX or vehicle (DMSO) for 18hr. Merged micrograph includes Mito-RFP and Bodipy 665/676 channels to demonstrate co-localization (white).

(B-C) Quantification of C2C12 transfected with non-targeting, FATP4, or PLIN5 siRNA followed by 18hr ISO-IBMX or vehicle treatment. (B) Colocalization of LDs with mitochondria was measured as % LD pixels overlapping with mitochondria, and (C) LD area/cell was measured, normalized to control. At least 33 cells were analyzed per condition across N ≥ 3 biological replicates. Error bars represent ± SD.

(D-E) C2C12 were assayed as described in Fig. 2A–B, following RNAi treatment using non-targeting, FATP4, or PLIN5 siRNA. (D) Red C12 incorporation into LDs following CM chase was measured, normalized to control cells. At least 9 cells were analyzed per condition across N ≥ 3 biological replicates. Error bars represent ± SD. (E) Red C12 accumulation into mitochondria relative to initial LD incorporation following HBSS starvation was measured, normalized to control cells. At least 9 cells were analyzed per condition across N ≥ 3 biological replicates. Data are expressed as means, error bars represent ± SEM.

(F) Proposed model of FA trafficking during starvation. Under basal conditions PLIN5 interacts with ATGL and CGI-58 leading to inhibition of lipolysis. During starvation: (1) PKA phosphorylates PLIN5 at S155; (2) phosphorylation of PLIN5 promotes lipolysis and release of FAs; (3) released FAs are channeled to mitochondria, where FATP4 converts FAs to Acyl-CoAs enabling; (4) transport into mitochondria for β-oxidation.

Cartoon created with Biorender.com.

Scale bar, 10 μm. *p < 0.05. **p < 0.01***p < 0.001.

See also Figure S5

Key Resources Table

REAGENT or RESOURCE	SOURCE	IDENTIFIER
Antibodies		
Rabbit monoclonal anti-FATP4	Abcam	Cat#ab2000353
Rabbit monoclonal anti-β-tubulin	Cell Signaling Technologies	RRID:AB_823664
Chicken polyclonal anti-GFP	Thermo Fisher	RRID:AB_2534023
Rabbit monoclonal anti-mitofusin-2	Cell Signaling Technologies	RRID:AB_2750893
Rabbit polyclonal anti-CPT1B	Abcam	RRID:AB_10712608
Bacterial and virus strains		
Escherichia coli BL21 (DE3) RIPL	FisherScientific	Cat#NC9122855
Chemicals, peptides, and recombinant proteins		
(−)-Isoproterenol hydrochloride (ISO)	MilliporeSigma	Cat#I6504
3-Isobutyl-1-methylxanthine (IBMX)	MilliporeSigma	Cat#I5879
GFP-Trap® magnetic agarose	ChromoTek	Cat#gtma
MitoTracker Deep Red FM	ThermoFisher	Cat# M22426
Oleic acid, [1-14C]-	Perkin Elmer	Cat#NEC317250UC
L-carnitine	MilliporeSigma	Cat#C0158
Bovine serum albumin, fatty acid free	MilliporeSigma	Cat#A8806
Lipofectamine 2000 transfection reagent	ThermoFisher	Cat#11668019
DharmaFECT	Horizon Discovery	Cat#T-2001-02
Fibronectin	MilliporeSigma	Cat#F2006
Bodipy 665/676	ThermoFisher	Cat#B3932
Bodipy 558/568 C12	ThermoFisher	Cat#D3835
n-dodecyl-β-D-maltoside (DDM)	GoldBio	Cat#DDM5
SUMO protease	ThermoFisher	Cat#12588018
Oleic acid	MilliporeSigma	Cat#O1008
Protease	MilliporeSigma	Cat#P8340
Phosphatase inhibitor cocktail 2	MilliporeSigma	Cat#P5726
Phosphatase inhibitor cocktail 3	MilliporeSigma	Cat#P0044
Critical commercial assays		
HiFI DNA Assembly Master Mix	New England Biolabs	Cat# E2621
Q5® Site-Directed Mutagenesis Kit	New England Biolabs	Cat# E0554S
KLD Enzyme Mix	New England Biolabs	Cat# M0554S
RNeasy Plus Mini Kit	Qiagen	Cat#74134
High-Capacity RNA-to-cDNA Kit	Applied Biosystems	Cat#4387406
SYBR Green PCR Master Mix	Applied Biosystems	Cat#4309155
Deposited data		
Proteomics data “PXD031591”	This paper	https://www.ebi.ac.uk/pride/
Experimental models: Cell lines		

REAGENT or RESOURCE	SOURCE	IDENTIFIER
Human: U-2 OS cell line	ATCC	HTB 96
Mouse: C2C12 cell line	ATCC	CRL 1772
Oligonucleotides		
ON-TARGETplus mouse PLIN5 siRNA SMARTPOOL	Horizon Discovery	Cat#L-055756-01-0005
ON-TARGETplus mouse FATP4 siRNA	Horizon Discovery	Cat#J-063631-12-0005
ON-TARGETplus non-targeting control pool	Horizon Discovery	Cat#D-001810-10-05
Primer: PLIN5 forward: CCATCTCGCCTATGAACACTCTT	Gallardo-Montejano et al.[37]	N/A
Primer: PLIN5 reverse: CAGCTGGGCCAGCATCTC	Gallardo-Montejano et al.[37]	N/A
Primer: 18S forward: GTAACCCGTTGAACCCCATT	Gallardo-Montejano et al.[37]	N/A
Primer: 18S reverse: CCATCCAATCGGTAGAGCG	Gallardo-Montejano et al.[37]	N/A
Recombinant DNA		
Mito-GFP	Jennifer Lippincott-Schwartz[66]	N/A
Mito-RFP	Jennifer Lippincott-Schwartz[65]	N/A
mApple-Sec61b	Jennifer Lippincott-Schwartz [67]	Addgene 90993
mOrange2-SKL	Michael Davidson[9]	Addgene 54596
mEmerald-C1	Michael Davidson[69]	Addgene 53975
ss-TagBFP-KDEL	Gia Voeltz[68]	Addgene: 49150
pEYFP-C1-PLIN5	Carole Sztalryd[4]	N/A
Em-PLIN5	This Study	N/A
PLIN5	This Study	N/A
Em-PLIN5CΔ (1-424)	This Study	N/A
Em-PLIN5CΔ (1-443)	This Study	N/A
Em-PLIN5CΔ (1-453)	This Study	N/A
Em-HP-PLIN5C (396-463)	This Study	N/A
Em-HP-PLIN5C (415-463)	This Study	N/A
Em-HP-PLIN5C (425-463)	This Study	N/A
Em-HP-PLIN5C (435-463)	This Study	N/A
Em-HP	This Study	N/A
Pex-Em	This Study	N/A
Pex-Em-PLIN5C (425-463)	This Study	N/A
Em-PLIN5 (S155E)	This Study	N/A
Em-PLIN5CΔ (1-424) (S155E)	This Study	N/A
PLIN5 (S155E)	This Study	N/A
PLIN5CΔ (1-424)(S155E)	This Study	N/A
Pex-Em-PLIN5C (425-463)	This Study	N/A
Pex-TagBFP	This Study	N/A
Pex-TagBFP-FATP4C(157-643)	This Study	N/A
ppSUMO-hPLIN5	This Study	N/A
ppSUMO-hPLIN5CΔ (1-424)	This Study	N/A

REAGENT or RESOURCE	SOURCE	IDENTIFIER
Software and algorithms		
ImageJ	NIH[72]	https://imagej.net/ij/index.html
CellProfiler	Stirling et al.[73]	https://cellprofiler.org/
TrackMate	Tinevez et al. [74]	https://imagej.net/plugins/trackmate/
Linear assignment problem tracking algorithm	Jaqaman et al.[75]	https://imagej.net/plugins/trackmate/algorithms
Zen 2	Carl Zeiss	https://www.micro-shop.zeiss.com/en/us/softwarefinder/software-categories/zen-blue/
Other		
Silica gel TLC plates	MilliporeSigma	99570